Hindawi
Journal of Chemistry
Volume 2023, Article ID 6338649, 22 pages
https://doi.org/10.1155/2023/6338649

Review Article

Multielement Doped Barium Strontium Titanate Nanomaterials as Capacitors

Balachandran Ruthramurthy,[1] **Kiflom Gebremedhn Kelele**,[2] **H. C. Ananda Murthy**,[2,3] **Kar Ban Tan**,[4] **Kah Yoong Chan**,[5] **Dhanalakshmi Muniswamy**,[6] **Aschalew Tadesse**,[2] **and Suresh Ghotekar**[7]

[1]*Department of Electronics and Communication Engineering, SoEEC, Adama Science and Technology University, Adama, P.O. Box 1888, Ethiopia*
[2]*Department of Applied Chemistry, School of Applied Natural Science, Adama Science and Technology University, Adama, P.O. Box 1888, Ethiopia*
[3]*Department of Prosthodontics, Saveetha Dental College & Hospital, Saveetha Institute of Medical and Technical Science (SIMATS), Saveetha University, Chennai 600077, Tamil Nadu, India*
[4]*Department of Chemistry, Faculty of Science, University of Putra Malaysia, Serdang 43400, Selangor, Malaysia*
[5]*Faculty of Engineering, Multimedia University, Cyberjaya 63100, Selangor DE, Malaysia*
[6]*Department of Physics, Nrupathunga University (Government Science College), N.T. Road, Bangalore 560001, India*
[7]*Department of Chemistry, Smt. Devkiba Mohansinhji Chauhan College of Commerce and Science, Silvassa 396230, University of Mumbai, Dadra and Nagar Haveli (UT), India*

Correspondence should be addressed to Balachandran Ruthramurthy; nribala@gmail.com

Received 3 June 2022; Revised 26 February 2023; Accepted 25 March 2023; Published 6 April 2023

Academic Editor: Ajaya Kumar Singh

Due to the growing demand of energy and wastage of energy, there exists an interest of storing energy so that it could be utilized efficiently. Capacitors are materials designed for such an application. Ferroelectric materials are known for their application as capacitors. Of such materials, perovskites are the preferable classes of materials that have been used as capacitors. Barium strontium titanate nanomaterial is a member of perovskites which encompasses a smaller dielectric loss, elevated dielectric constant, and good thermal stability. Research studies also clarified that incorporating dopants into a barium strontium titanate nanomaterial of high dielectric materials including metal/metal oxides enhances their efficiency and effectiveness. Moreover, multielement doping or codoping has shown better dielectric properties as compared to the unidoping of BST. In this review, barium strontium titanate capacitors codoped with more than one metal/metal oxides have been studied most of which have shown that the codoped barium strontium titanate materials possess improved and sufficient dielectric properties to be utilized as capacitors. We believe that this work will have of its own contribution on understanding the doped barium strontium titanate nanomaterial by clarifying the most probable and detail reasons behind the enhancement of dielectric properties of codoped barium strontium titanate nanomaterials.

1. Introduction

The high-level consumption of traditional fuel energy and the ongoing elevation of demands for energy have become a big concern where loss of energy is simultaneously observed, leading a way to develop environmentally-friendly energy sources and storing mechanisms [1–4]. Hence, studies on renewable energy initiate the preparation of energy accumulating devices such as batteries, electrochemical capacitors, and dielectric capacitors [5, 6].

A variety [1] of materials possesses a variety of energy and power accumulation capacity due to variable techniques

of energy accumulation as well as charging-discharging processes [7]. For instance, batteries possess enhanced energy accumulating capacity and comparatively lower power density as a result of the delayed charge transporters flow during the charging-discharging step [8]. On the other hand, electrochemical capacitors possess enhanced power density and longer charging-discharging time (in seconds) during their utilization [7]. Batteries are being highly applied and favoured by charge storing devices. But for massive energy production as well as a large amount of power, capacitors have been found as the preferable devices [9]. Out of these, solid-state dielectric devices utilized as energy accumulating capacitors of minimized size (mostly at nanoscale) are gaining much interest because of their popular pulsed power technology utilizations. Ferroelectrics (FE) as well as antiferroelectrics (AFE) have been found as suitable materials for the pulsed power capacitors because of the enhanced energy-accumulating capacity and better charge-discharge characteristics relative to ferroelectrics and dielectrics [10–16].

The performance of a charge and energy storage system is affected by two factors: the amount of energy that is stored in a system (volumetric energy density or specific energy) and the speed where energy is either added or released from it (power density or specific power) [17]. Batteries, fuel cells, capacitors, and supercapacitors have different combinations of power density and energy density which is illustrated in Figure 1.

The measured electrical energy accumulated by a device is expressed through its respective capacitance. Capacitance is used to derive the dielectric constant value of a device or a sample, which refers to a measurement of amount of polarization of a sample. It is affected by content, growth steps as well as the crystal arrangement of the sample. The dielectric constant is the ratio of electrostatic energy accumulated around a unit volume per unit potential rise. It is expressed as follows:

$$\varepsilon_r = \frac{Cd}{\varepsilon_0 A}, \tag{1}$$

where ε_r refers to dielectric constant, C refers to capacitance, d refers to thickness, and A and ε_0 refer to a material surface area and permittivity of free space, respectively [18, 19].

Three classifications of capacitors are known which include electrostatic, electrolytic, and a supercapacitor. An electrostatic capacitor possesses a dry separator, extremely less capacitance which is primarily applied in changing radio frequencies as well as filtering. It encompasses a size range in between picofarads (pF) and small microfarad (μF). An electrolytic capacitor has elevated capacitance as compared to an electrostatic capacitor where its accumulating capacity is at the microfarads range. It has a watery separator which is utilized for filtering, buffering, and signal coupling. Supercapacitors store enormous quantities of electrical charge and frequently involve short charge and discharge period at elevated current. They have the unique advantages of enhanced power density and durability, small mass, and a higher heat scope of −40°C to 70°C [9, 20].

Capacitors are composed of an electrolyte, two electrodes, and a separator (dielectric material) that isolates the electrodes electrically which is inserted in between the electrodes, as can be seen in Figure 2. Capacitors use sample materials full of porosity, as separators, so as to accommodate ions and ultimately store electrical charge. Electrodes are the most crucial and fundamental constituent of capacitors. As a result, the efficiency of capacitors relies on the electrochemical behaviour of electrodes, the range of voltage applied as well as the electrolyte solution [21–24]. Capacitors are being applied in fuel cell automobiles, hybrid vehicles of less emission, electric automobiles, forklifts, and weight cranes [25].

Obviously, charge accumulated by the capacitor, Q, is expressed via the following equation:

$$Q = C\,x\,V. \tag{2}$$

Here, C refers to capacitance, while V corresponds to the applied potential.

Meanwhile, capacitance of a parallel plate capacitor is expressed as follows:

$$C = \varepsilon_0 \varepsilon_r \frac{A}{d}. \tag{3}$$

Here, ε_0 corresponds to free space permittivity (8.854×10^{-12} F/m), C refers to capacitance (F), ε_r belongs to a dielectric constant (F/m), A corresponds to a plate cross-sectional area (m^2), and d refers to thickness of a dielectric layer (m).

Meanwhile, the normalized dielectric loss or loss tangent is determined by the corresponding distribution of the imaginary permittivity, ε'', and an actual relative permittivity, ε', using the following simple equation [26]:

$$\tan\delta = \frac{\varepsilon''}{\varepsilon'}. \tag{4}$$

The dielectric loss, D, is also determined from the capacitance and resistance of parallel plate capacitors using the following formula:

$$D = \tan\delta = \cot\theta = \frac{1}{2\pi f C_P R_P}. \tag{5}$$

Here, δ refers to a loss angle; while θ refers to a phase angle, f refers to frequency, R_P belongs to an equivalent parallel resistance, and C_P also refers to a respective capacitance.

Generally, an enhanced energy-accumulating property of a capacitor is expressed through higher recoverable energy density (W_{re}), larger energy efficiency (η), a speedy charge-discharge process, higher current density (C_D), and larger power density (P_D). These parameters are determined through the following equations [27, 28]:

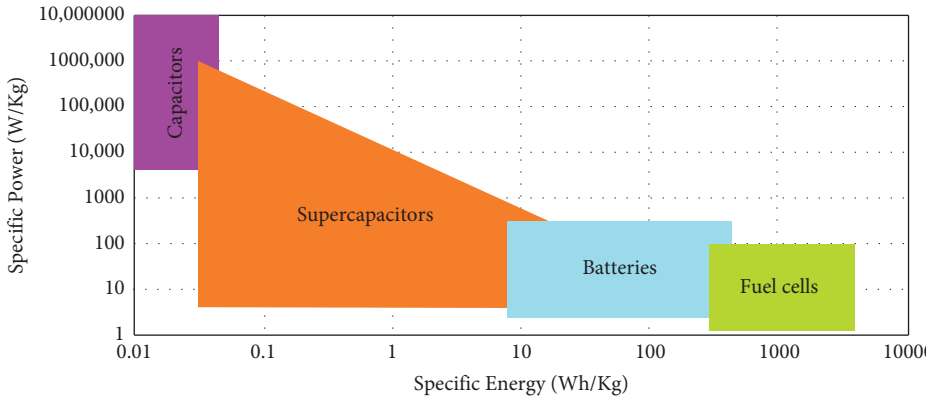

Figure 1: Specific power as well as energy of a variety of devices.

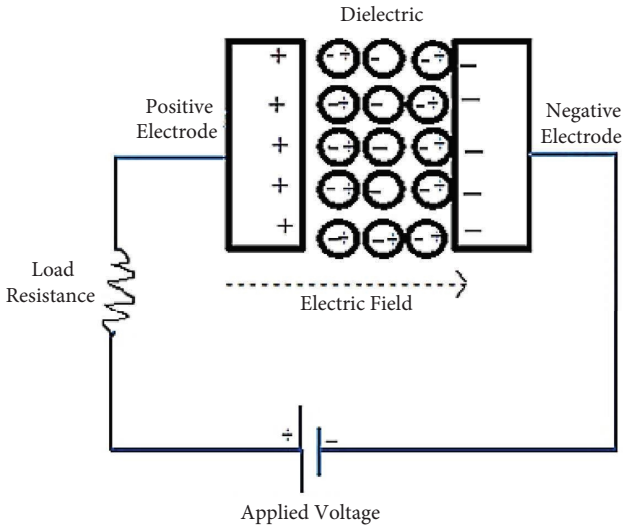

Figure 2: Schematic of the conventional capacitor.

$$W_{re} = \int_{P_r}^{P_{\max}} EdP,$$

$$\eta = \left(\frac{W_{re}}{W_{re} + W_{\text{loss}}}\right) 100\%, \tag{6}$$

$$C_{D\max} = \frac{I_{\max}}{S},$$

$$P_{D\max} = \frac{EI_{\max}}{2S}.$$

Here, E represents an applied field, P_r corresponds to the remnant polarization, $P_{\max}$ refers to saturation polarization, W_{loss} refers to the loss energy density, C_{Dmax} refers to the maximum current density, P_{Dmax} represents a peak power density, $I_{\max}$ refers to a maximum current, and S represents an electrode area [29–31].

The energy, E, accumulated at a capacitor is directly related to the capacitance, that is,

$$E = \frac{1}{2}CV^2. \tag{7}$$

Here, C represents the capacitance, while V refers to an applied voltage [29–31].

As a general fact, power is also the ratio of energy spent to unit time. The internal parts of capacitors such as the current collector, electrodes, and dielectric material affect the resistance that is determined together with the equivalent series resistance (ESR). A voltage obtained during discharging is calculated by such resistances. At a fitting impedance ($R = \text{ESR}$), the maximum power, $P_{\max}$, of a capacitor is expressed through the following equation:

$$P = \frac{V}{4}\, x\, ESR, \tag{8}$$

where ESR controls the maximum power of a capacitor [29–31].

To elevate charge-storing characteristics of a capacitor, its capacitance needs to be increased. This is possibly done through lowering of a dielectric thickness. However, conventional dielectric materials, such as SiO_2, decreasing dielectric thickness results in an increased leakage current. The other possibility is increasing the cross-sectional area of the capacitor which is difficult to fabricate such structures due to the enormous size. The ultimate option is therefore using a material with a higher dielectric constant [21]. Nanomaterials with higher dielectric constant have been utilized in the electronic device industry to a larger extent. Perovskite oxide ferroelectrics, ABO_3, are being used as higher dielectric constant materials during the preparation of capacitors. They are highly affected by inner resistance, the oxidation state of an element at the *B-site*, and surface area. Perovskite nanomaterials, such as $BaTiO_3$, $SrTiO_3$, and barium strontium titanate (BST), have possessed suitable properties which make them become perfect candidates for many energy storage applications [32–37]. Meanwhile, doping involves significant effects on a dielectric property and capacitive application of BST nanomaterials. More specifically, doping with multielements at a time has an even higher impact on improving the performance of BST as

a capacitor. BST nanomaterials have been doped with a variety of single elements (unidoping) and multielements (co-doping). Therefore, this review is aimed at pointing out the specific effects of codoping on BST nanomaterial dielectric property and capacitive application as well as exploring the possible detailed mechanisms by which the changes were obtained.

1.1. Dielectric Properties of BST Nanomaterial. BST is a metal oxide dielectric substantial sample where more focus has been given to it as a result of the small dielectric loss, elevated dielectric constant, good thermal stability, adjustable cure temperature, and high breakdown field strength properties possessed by it. BST belonging to perovskite materials has a typical perovskite arrangement of atoms [38–41], as is observed in Figure 3.

BST nanomaterial has shown its own dielectric properties which make it to be the right candidate for a variety of capacitor-containing materials. For instance, a report by Balachandran et al. has explored the dielectric parameters of BST synthesized through the gradual injection sol-gel method. A dielectric constant of 1,164 Pa/cm^2, a leakage current density of 49.4 Pa/cm^2, and a dielectric loss of 0.063 Pa/cm^2 have been observed when calcined at 800°C and sintered at 1,350°C [42]. Baniecki et al. also reported a BST thin film used as a capacitor in a small inductance decoupling utilization where the capacitance density was reported as 1.2 μF/cm^2. The leakage current density has been found lower than 10^{-9} A/cm^2 during an applied voltage of 2 V, while the breakdown field was observed as higher than 2.5 MV/cm at 20°C [43]. Before ten years, a work on BST thin film used as a capacitor has reported that they have been used in microwave utilizations with a dielectric loss range of 0.003–0.009 [44]. Another work by Balachandran et al., reported work on dielectric characteristics of BST-based metal insulator metal capacitors for DRAM cell where silver was used as upper as well as a lower electrode. Kumari and Dasgupta Ghosh have synthesized BST through doping of barium titanate by strontium during a sol-gel method. They have reported that the storing capacity of BST nanoparticles which was expressed by its dielectric constant was found at its maximum value of 4,915 while its dielectric loss was as low as 1.91 [45]. A cubic structured BST nanomaterial was synthesized through a polymeric precursor method using citric acid as well as ethylene glycol, for the first time, by Arya et al. A dielectric constant of 190 and dielectric loss of 0.001 at 500°C and 100 kHz have then been reported [46]. There was also a report by Zhang et al. where BST thin film over the surface of platinum has been synthesized through an electrophoretic deposition method and was investigated for its capacitive nature. It possessed a dielectric constant as well as dielectric loss of 3,446 and 0.011, respectively, at 10 kHz and at room temperature. Therefore, reports have confirmed that BST nanomaterial has possessed sufficient dielectric properties which help it to be utilized as a capacitor in a variety of energy storing devices [47].

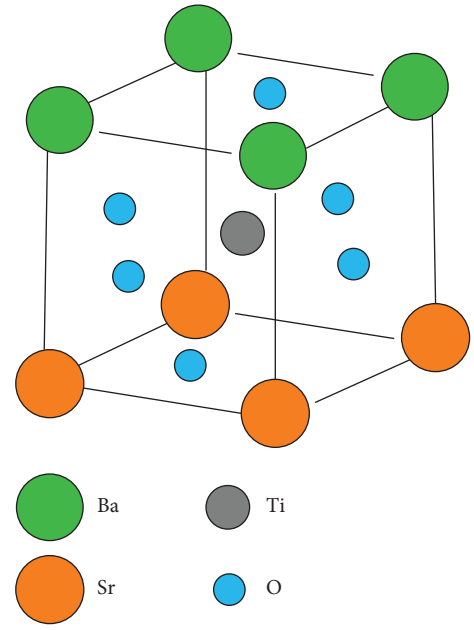

Figure 3: Nonpolar structure of BST at the room temperature.

1.2. Effect of Unidoping and Codoping on Dielectric Property of BST Nanomaterial. The dielectric behaviour of BST is modified by varying and managing the ratio of Ba to Sr as well as a limited exchange of cations at the *A*- as well as *B-sites* of its ABO_3 structure through doping. Reports also clarified that the parameters of dielectrics such as dielectric constant, dielectric loss, and leakage current do usually get affected by the synthesis technique, chemical content, microstructure, identity, and the amount of dopants added where acceptor (lower valance than *A* or *B* components) and donor (higher valance than *A* or *B* components) dopants effectively change the properties of BST nanomaterial [18, 48–55]. Acceptor ions easily substitute Ti at the *B-site* where a one-phase arrangement is formed that leads to extra ionization of dopants which results in the occurrence of vacancies as well as lattice irregularities [56, 57]. Dopants generally alter the physicochemical as well as charge carrier characteristics of the BST due to the formation of oxygen vacancies. These vacancies usually result in higher oxygen diffusion rates as the transport lengths are lowered which ultimately changes the specific capacitance of BST nanomaterial [58]. During the synthesis process of BST nanomaterials, larger temperature annealing in the air (slightly reducing ambient) is a common task where intrinsic oxygen vacancies ($V_O^{\bullet\bullet}$) are generated. They are expressed by the following equation [59, 60]:

$$O_0 \longrightarrow V_O^{\bullet\bullet} + 2e + \frac{1}{2} O_2 \uparrow. \tag{9}$$

On the other hand, the reduction from Ti^{4+} to Ti^{3+} also causes additional oxygen vacancies to appear. As a result, a leakage current is usually increased which diminishes dielectric parameters of a dielectric which hinders the application of BST nanomaterial devices. This problem is usually solved through ion substitution [61–63]. The charge-

compensating heterovalent replacement of Ti^{4+} ions of BST resulted in the formation of complex defects which subsequently trapped the electrons in a motion. This invites lowering of dielectric loss along with leakage current as well as a dielectric constant elevation. Therefore, complex-defect design is utilized in enhancing the dielectric constant and capacitance of a capacitor [64–66]. Therefore, the addition of single dopants to the BST base material is effective in improving the capacitive application of the BST nanomaterial. This has primarily resulted from the formation of defects such as oxygen vacancies following the incorporation of the dopants and replacing the *A*- and/or *B*- sites of the BST perovskite structure. It is also caused by further ionization of the dopants after they obtain electrons from the Ti^{4+} component of BST. Hence, doping is considered to be one of the successful methods employed to advance the utilization of BST as a dielectric material in capacitors.

These days, scholars are performing a significant number of research studies on unidoped BST materials where the dielectric properties and capacitive nature of BST have been enhanced. Hence, there have been many suggestions given for the mechanism of how the dopants affect the microstructural as well as electrical characteristics of the BST material. For instance, Mn doping involves the trapping of electrons which lowers the dielectric loss being an acceptor-class impurity located on the grain boundaries [67, 68]. Attar et al. reported work on dielectric characteristics of BST nanopowder doped with Bi prepared through the sol-gel technique where the dielectric constant has been observed increasing to a maximum value at a temperature of 80°C, due to enhancement of the grain size and was then lowered above the Curie temperature. Meanwhile, the dielectric loss decreased as a result of balancing of the oxygen vacancies formed by doping, through reduction of free electrons. The highest amounts of both dielectric constant and dielectric loss were lowered during elevation of Bi concentration [69].

A report by Eswaramoorthi et al. explored the changes in electrical characteristics of BST thin film by Ga which was incorporated as a dopant. As a result, both the dielectric constant as well as dielectric loss was lowered as the Ga concentration was increased. The dielectric constant was observed decreasing due to the reason that the dipoles hardly pursue an enforced field and lowering of particle size of BST after the addition of Ga. Introduction of Ga to BST has resulted in the lowering of dielectric loss as Ga^{3+} attracted as well as neutralized bouncing electrons found within various Ti^{4+}. On the other hand, Ga has an ionic radius of 0.62 Å, while Ti has 0.61 Å ionic radii which are about identical, and hence, ions of Ga^{3+} are expected to take up the space initially occupied by Ti^{4+} ions found at the B-sites of ABO_3 which behaves as an electron collector [70].

$Ba_{0.7}Sr_{0.3}TiO_3$ in the form of ceramics doped with Ni synthesized through the slow-injection sol-gel technique had a minimum dielectric loss equal to 0.02 and a 1,603 dielectric constant value. The dopant Ni occupied site B of the arrangement, and Ni^{2+} substituted Ti^{4+} site where oxygen vacancies were formed which reduced the dielectric loss. An increase in sintering and calcination temperature is also another driving force for the lowering of the dielectric loss. When computed with BST, the dielectric constant of Ni doped BST ceramics has been found higher. This is the result of conduction state formation around grain edges [71–73]. Similarly, a report by Novianty et al. has revealed their finding where the addition of the dopant Ta_2O_5 into $Ba_{0.5}S_{0.5}TiO_3$ caused the value of the dielectric constant to be increased. Ta_2O_5 increased the number of donor dopants. This derived elevation in the amount of negative charge carrier content and inner electric potential. Hence, all these changes make the depletion region grow larger. Ultimately, BST doped with Ta_2O_5 in the form of thin films shown improved dielectric characteristics as compared to pure BST [74]. Another work by Chen Zhang et al. has shown that as Sb_2O_3 content was increased, the dielectric constant elevated at first which later lowered. Dielectric loss of the BST, on the other hand, has been found elevated. These phenomena are due to the formation of vacancies and defects after the *A*- and *B*-sites of the BST were occupied by the Sb^{3+} ions [75]. The effect of zircon on the dielectric property has been investigated where the replacement of Ti^{4+} by Zr^{4+} ions caused a dielectric constant increment as well as dielectric loss lowering. However, these were due to the enhancement of frequency stability [76].

A report on the impact of gold over some properties of BST by Wang et al. has explored the improved properties of BST. Increased crystallization, lower leakage current density, and enhanced dielectric constants have been observed as a result of doping of the BST with gold. When the dopant gold was introduced to BST, it catalyzes nucleation of the BST nanoparticles and enhances their crystallinity. This resulted in an elevation of the grain size which resulted in higher dielectric constants and lowers leakage current as compared to the pure BST. According to this report, the grain size and dielectric constants values are directly proportional [77].

In contradiction to many reports, doping $Ba_{0.6}Sr_{0.4}TiO_3$ BST with iron has resulted in decreased dielectric constant value relative to the pure BST. But no adequate reason and explanation have been given to this unusual result [26]. Meanwhile, another report on the Fe doped $Ba_{0.5}Sr_{0.5}TiO_3$ BST synthesized through slow rate injection sol-gel has shown expected results where the dielectric constant value of doped BST has elevated as a result of increment in Fe concentration, starting at 0.1 to 1 mol % while the sintering temperature was increased. But the dielectric loss was observed decreasing which is mainly caused by the evolution oxygen vacancies, lowering of oxygen, and appearance of space charge polarization by an electric potential. Meanwhile, the dielectric constant was elevated when the sintering temperature was increased and got lowered when the calcination temperature was elevated. On the other hand, the dielectric loss has shown higher values as calcination temperature was elevated. It was lowered as a result of the elevation of sintering temperature [78].

Hence, it was described that the addition of dopants to BST might not always result in enhancement of the dielectric parameters and capacitive application of BST at any condition, rather there are optimized values of calcination temperature and the amounts of dopants. On the other

hand, increment in sintering temperature brings about advancement of the capacitive utilization of the doped BST samples.

As can be observed from the previous reports, unidoping resulted in an enhanced dielectric property of BST. However, more enhancements in the dielectric property of BST and its capacitive application can be obtained using codoping or multielement doping of the BST. These days, multielements codoping has got more focus since it enhances the surpassing dielectric properties that are difficult to be achieved by either single *A*-site or *B*-site doping. There exist two ways of codoping: one way is doping the *A*- as well as *B*-sites with variable elements; the second way is doping the *A*- or *B*-site with varied elements [79]. When BST is codoped with more than one dopant, the radius is taken as a major factor for the site where dopants are added. The *A*-site containing Ba^{2+} (1.35 Å) and Sr^{2+} (1.15 Å) is preferably substituted by the dopant with a higher ionic radius, while Ti^{4+} (0.68 Å) are replaced by the smaller dopant [80–82]. To obtain a capacitor of minimum dielectric loss, elevated tunability, and solve the synchronous alternation of dielectric properties, methods such as compositing or forming heterojunctions using complementary components and codoping are usually practiced [83–86]. Codoping has usually been used as a better and efficient way of increasing the dielectric properties of BST. It solves some of the problems faced during unidoping where enhancement of a dielectric parameter occurs along with lowering in other ones. Doping of BST sometimes results in elevation of the dielectric constant along with the leakage current. It might also end with a reduced dielectric constant and leakage current. This could be due to the occurrence of a paraelectric hexagonal phase which is visibly observed when the amount of the dopant added is higher. It then results in Jahn–Teller distortion which hinders the real utilization of BST capacitors. On the other hand, unidoping leads to the formation of oxygen vacancies that lower the dielectric property of BST. Hence, codoping notably prevents the formation of the hexagonal phase and lowers the number of oxygen vacancies. On the other hand, elements of the codopant act as a donor and acceptor dopant at a compensated concentration [48, 87–96].

The advantage of codoping over unidoping, in enhancing the dielectric properties of BST, has been clearly observed when BST was doped with K^{+1} and Mg^{2+} ions through a sol-gel method. The dielectric constant became greater than BST for the K^{+1}/Mg^{2+} ions codoped BST by a larger value relative to the K-doped BST as well as Mg-doped BST. Dielectric loss of the BST sample has gone to a minimum value for the K^{+1}/Mg^{2+} ions codoped BST than for the K-doped BST as well as Mg-doped BST. The K^{+1}/Mg^{2+} ions codoped BST film possessed larger density and small amount cracks which made it to own enhanced dielectric properties. On the other hand, while the codoped BST is heated at elevated temperature, O^{2-} found at the BST lattice is removed as O_2. This results in one oxygen vacancy and two free electrons. The electrons are easily absorbed by the K^{+1} and Mg^{2+} ions which lower the carrier concentration as well as dielectric loss. After the K^{+} ions substituted the Sr^{2+} and Ba^{2+} ions, the Ba/Sr ratio has been elevated which resulted in increased dielectric constant [97].

Multielement doping has an impact of on the microstructure and electrical properties of BST thin film. Such a phenomenon has been clearly observed when BST was codoped with Ce^{3+}/Mn^{2+} ions in a work by Qian et al. Elevated capacitance along with a higher dielectric constant and a lower dissipation factor of a codoped BST capacitor was obtained. This is mainly due to the formation of defect complexes of $Ce'_{Ti} - V_O^{\bullet\bullet}$ or $Mn''_{Ti} - V_O^{\bullet\bullet}$ which lower the number of free oxygen vacancies and decrease the leakage current. Particle size of the BST was also lowered after the addition of the codopants, Ce and Mn. This brings about a higher volume fraction of grain boundaries which increased the length of conduction paths and lowered the leakage current [98]. In analogous to this report, impact of codoping on the dielectric characteristics of BST nanomaterial has also been observed when BST was codoped with Bi and Li according to a report by Alkathy et al. Dielectric constant has increased as a result of the space charge polarization in between grain boundaries that derives a potential barrier and free electrons obtained after the replacement of the Ti^{+4} ion by Li^{+1} ion. The acceptor-donor defect complex was formed after the replacement of Ba^{+2} ion by Bi^{+1} ion and that of Ti^{+4} ion by Li^{+1} ion. This produced an electron-pinned defect dipole where the hopping electrons were accumulated and attached at the defects. Hence, the dielectric loss has been reduced to a smaller value [99]. The same reasoning has been used to clarify the enhancement of dielectric permittivity of (Al, Nd) codoped BST [100].

As reported by Singh, codoping has the advantage of altering a dielectric parameter without affecting the other properties of the BST nanomaterial. Codoping of perovskites involves the formation of holes, electrons, and oxygen vacancies. Moreover, this results in an enhanced conductivity through the hopping of electrons among the ions of the dopants [101]. Such a phenomenon has been observed when BST was codoped with Ba ($Mn_{1/3}Nb_{2/3}O_3$) (BMN) in a report by Alema and Pokhodnya. The dopants have surprisingly lowered the dielectric loss up to 38% where tunability of the BST nanomaterial film has not been affected. This is due to the balancing act of the small Nb^{5+} on the tunability effect of large Mg^{2+}, during which both ions replaced Ti^{4+} ions. Coupling of Mg''_{Ti} as well as $V_O^{\bullet\bullet}$ charged defects reduced dielectric loss of the film through the removal of electrons at hopping among Ti^{4+} ions due to the variation of valance state of the dopants. Such a phenomenon also resulted in the reduction of leakage current of BST. The dielectric constant has been lowered due to the lowering of grain size after Mn and Nb were added to BST [102, 103]. The doping process of BMN is possibly represented by

a defect reaction known as Kroger–Vink notation which is expressed in the following equation [104]:

$$3Ba\left(Mg_{1/3}Nb_{2/3}O_3\right) + BaO \xrightarrow{T} iO_2 \;\; 4Ba_{Ba}^{x} + Mg_{Ti}^{''} + 2Nb_{Ti}^{\cdot} + 10O_O^x. \tag{10}$$

Almost opposite to this report, Xiaofeng et al. have shown that adding Mn, La, along with Nb dopants to BST, resulted in the substantial increase of dielectric loss which has been sharply lowered when the amounts of Mg, Fe, and Al were elevated. There was also an observation that the preliminary results of Mn-doped BST ceramics deviated in relation to earlier works by a larger extent [48].

Sometimes, codopants might enhance the dielectric constant which could still be lower than the pure BST. Such a case has been observed when Stemme et al. were studying the impact of fluorination of Fe-doped BST thin films on the number of oxygen vacancies. Fluorine acted as a donor codopant, while iron acted as an acceptor dopant so that electroneutrality is kept where the holes are filled by F^- ions and electrons taken by Fe^{3+} ions. The highest permittivity or dielectric constant value of 535 ± 12 has been obtained for the BST nanomaterial. Moreover, it was reduced to 348 ± 5 after BST was first doped with Fe due to distortion of the perovskite structure and the formation of defect dipoles by the internal bias field. But in the end, the value has been elevated to 398 ± 11 when fluorine was added as a codopant to the annealed Fe-doped BST. This is the result of the movement of the F^- ions into the oxygen vacancies [105].

Codoping is expected to lower the leakage current density to its lowest value as compared to unidoping. A decrease of leakage current densities from 2.79×10^{-7} A/cm^2 of pure BST nanomaterial to 1.23×10^{-7} A/cm^2 through efficient lowering of the charge carriers and formation of oxygen vacancies has been observed when BST was codoped with Mn and Y in a report by Liu et al. Lowering of dielectric loss to a minimum value of 0.0073 at 1 kHz was also observed [106]. Here, the acceptor dopant (Mn) diminished the negative charge carriers, electrons, while the donor dopant (Y) usually lowered the positive charge carriers, oxygen vacancies. Preheating decreased the amount of organic substances which cause leakage current densities. As a result, the amount of leakage current densities got lowered [107, 108]. In a similar way, the leakage current density of BST has been lowered when La and Co codopants added to BST through a metalorganic solution deposition method as reported by Zhang et al. This is the result of decreasing of the intrinsic oxygen vacancy by the La donor dopant through the formation of the cation vacancy [109].

On the other hand, a study on dielectric characteristics of BST codoped with La_2O_3 as well as Sb_2O_3 has found that the ions La^{3+} ions, as well as Sb^{3+}, occupied *A-sites* of the perovskite structure. BST doped by La_2O_3 has shown a large dielectric constant, which is higher than 4,500, which helps them to be proved candidates for the capacitor applications. An increase in La_2O_3 doping content also resulted in the lowering of dielectric loss as a result of replacement of *A-sites* in BST perovskite structure by the rare earth ions. It is due to the fact that electrons generated during the doping process were trapped by Ti^{4+} ions causing the formation of Ti^{3+} ions and the deoxidization of Ti^{4+} ion. Elevation of a dielectric constant has been observed as crystal lattice is shrinked and consequently, the lattice structures have also been deformed. At higher content of Sb_2O_3 concentration, the separation length of the centre ion to the nearest octahedron neighbours becomes shorter where the motion of Ti^{4+} ions gets confined. As a result, the unforced polarization of grain structure got weakened. Hence, both dielectric loss and dielectric constant were lowered [19].

Sometimes, codoping might not produce the expected sharp elevation of the dielectric characteristics of the BST nanomaterial. A study by Gao et al. dealing with the impact of Bi_3NbZrO_9 on the dielectric characteristics of BST ceramics has explored that the addition of more Bi_3NbZrO_9 resulted in enhancement of dielectric constant first which got lowered later and has finally shown a little increment. This is due to the formation of strontium vacancies at the *A-site*, as a result of the substitution of three Sr^{2+} ions by two Bi^{3+} ions. This drove the free movement of titanium ions and easy polarization. The dielectric loss became low at first which then got higher and higher constantly. Replacement of the Ti^{4+} ions by Nb^{5+} and Zr^{4+} ions resulted in lowering of the space in between anion and cation of oxygen octahedral where a higher amount of repulsion between oxygen ions has occurred. Therefore, the extent of polarization became lower [110]. The same codopants have been employed in another report, but different results have been obtained due to the variation in the synthesis method and conditions. Codoping BST nanomaterial with Mn and Y has resulted in dielectric constant, dielectric loss, and leakage current values which have been simultaneously impacted through the introduction of Mn and Y codopants. The dielectric constant value of the BST nanomaterial reached its possible maximum value as a result of enhanced crystallization at an annealing temperature of 750°C and 400 kV/cm applied voltage. Meanwhile, the dielectric loss lowered due to the formation of a higher amount of charged defects. The leakage current density has been similarly reduced. This is caused by the acceptor property of Mn and Y that replaced Ti, the lowering of electron density, and enhancement in crystallinity of the BST thin film. Besides these effects, codoping of BST with Mn and Y has also resulted in enhanced remnant polarization value. This is due to the increment of defect concentration as a result of a reaction between Y^{3+} ions and oxygen vacancies. Ultimately, polarizability or ferroelectric characteristics of the BST have been enhanced which matches with elevation of the dielectric constant [111].

Multielement doping also has effects on the conductivity of BST ceramics. Deepa et al. reported that the addition of Ag together with $50PbO : 30B_2O_3 : 20SiO_2$ dopants into BST has improved the dielectric and conductivity of BST. This is due to the lowering of the space between the dopant particles which led to lowered multipolar interaction among the particles. However, this caused the free motion of electrons over a large range of areas where an applied field existed. Hence, a radical elevation of dielectric constant as well as conductivity has been observed [112]. But this is not always true. A report by Bomlai et al. has shown that conductivity of BST has been decreased after 0.08 mol% MnO_2, 3 mol % SiO_2, and 3 mol % SbO_2 are added as codopants to BST during the synthesis of Sb, Mn-codoped BST ceramics containing TiO_2, and SiO_2 sintering additives through a conventional mixed-oxide process. The resistivity has been increased from 48 to 911 Ω-cm. The codopant Mn acted as an acceptor by replacing the Ti of BST where the charge density from the trapped electrons was elevated. This enlarged the barrier height which caused the conductivity to get lowered [113].

Grain size has variable effects over the dielectric characteristics of BST capacitors. It is sometimes directly proportional and other times inversely proportional with them. For instance, the elevation in grain size has been resulted in enhancement of relative permittivity to 419 and lowering of dielectric loss when BST was codoped through incorporation of cobalt along with fluorine in a report by Friederich et al. However, the reason behind the results was not adequately explained [114]. The same result has been obtained in another report dealing with the sintering properties and dielectric nature of B_2O_3/CuO codoped BST [115]. The increase in grain size has also been resulted in increasing the dielectric constants of Cu-F codoped BST, Fe-F codoped BST, and Co-F codoped BST as reported by Zhou et al. Here, F^- ions fill the oxygen vacancies found at the B-site which were obtained after the replacement of Ti^{4+} by Cu^{2+}, Co^{2+}, and Fe^{2+}. There upon, the internal field was reduced leading to the elevation of the dielectric constants [116].

Codoping has its own response to another characteristic parameter of dielectric materials, the Curie temperature T_c. In a report by Liang et al., the Curie temperature of BST nanomaterial has been reduced after the codopants Mn and Co were added to it. This is the result of the replacement of Ti of BST by Mn^{2+} and Co^{3+} ions which formed oxygen vacancies. Consequently, the vacancies were followed by the rupture of Ti-O chains which derived reduction of T_c of the codoped BST [117]. Similarly, lowering of Ba/Sr ratio of BST matrix has been resulted in lowering of T_c from −57.5 to −142°C after doping BST with $MgMoO_4$. Unlike many other works, codoping has also shown lowering of dielectric constant of BST. Here, elevation of $MgMoO_4$ content caused the dielectric constant to lower steadily. This is caused by the smaller dielectric constant values of both $MgMoO_4$ ($\varepsilon = 7.07$) and $BaMoO_4$ ($\varepsilon = 9.3$) [118]. Likely, doping of $(Ba_{0.74}Sr_{0.26})$-TiO_3 with La and Sb has resulted in lowering of T_c from 23°C to a value lower than −25°C as the maximum amount of 0.8 mol % of Sb_2O_3 and 1.6 mol % La_2O_3 was added to the ceramics through a solid state method [19]. In contradiction to this report, the Curie temperature was elevated to larger temperature when BST was codoped with a glass containing PbO-SiO_2-B_2O_3 according to a report by Zhang et al. It has been reported that after the addition of codopants into BST, the compositional variation in the ferroelectric material was observed. Mainly, the formation of $PbTiO_3$ is responsible for the steady increment of T_c. $PbTiO_3$ has a T_c value of 485°C which is greater than the value for BST (120°C) [119]. T_C of BST has been observed first elevated which was then lowered when codoped with 2.0 wt % Mg as well as 2.0 wt % Mn through a solid-state reaction method. According to Zhang et al., this was due to the lowering of the internal stress and microstructural change from cubic to hexagonal [120].

It is known that the phase transition temperatures, T_c, of the codoped BST samples explore the temperature at which a maximum dielectric constant value is obtained. It is used to determine the amount of the codopants needed to make the BST sample to be a better capacitor. For instance, the Bi_3NbZrO_9-doped BST has shown a varied T_c as the amount of the codopant was fluctuated. Elevation of Bi_3NbZrO_9 from 0.5 wt. % to 5 wt. % has lowered the T_c value from −10.8°C to −57.2°C. Here, elevation of the dopant amount resulted in enhancement of the number of Bi, Zr, and Nb ions which are going to be incorporated to the BST lattice. However, this became the deriving g force for the lattice distortion, lowering of volume of the crystal cell, reduction of the gaps between oxygen octahedrons, and prohibiting the motion of Ti ions. Hence, decreasing of long range static force, increasing of the potential well depth, as well as lowering of heat of transformation were observed. These all caused the phase transition temperature to be lowered [110]. The extent of variation of T_c with the amount of dopant incorporated to a BST sample is useful to perfectly predict the type of application where the doped BST is going to be utilized. 0.5 mol % Mn and 1.0 mol % Y-codoped BST ceramics has shown no lowering of T_c, and this made it to be an appropriate material for a pyroelectric application. Its T_c has been found as ~25.38°C which belongs to a phase transition from paraelectric to ferroelectric [121]. In a report by Hu et al., a T_c value of 305 K has been recorded for a phase transition of ferroelectric phase to a paraelectric one when BST was doped with 0.5 wt % B_2O_3 [122].

On the other hand, codoped BST materials possess dielectric constant values which vary with temperature. Jiang et al. reported that a BST codoped with 2.5 mol % B_2O_3 and 2.5 mol % CuO synthesized using a solid-state reaction route at a sintering temperature of 950°C has shown elevation of dielectric constant value with increasing temperature of the process starting from the smallest value of ε equal to 7.4. Such a phenomenon is the result of increase in density as well as grain size [115]. Similarly, in a research work reported by Wang et al., enlargement of crystallization temperature from 850°C to 1,000°C has been resulted in the enhancement of dielectric constant, starting at 119 all the way to 317, during codoping of BST with $BaAl_2Si_2O_8$ to produce a BST ceramics possessing the 3.0 J/cm^3 highest energy density. This value is recorded as a larger value as compared to the classical capacitor making the $BaAl_2Si_2O_8$ codoped BST [123]. In the same trend, incorporation of 2, 4, and 8 mol %

Bi and Li codopants to BST through a solid-state reaction method has resulted in an elevated dielectric permittivity in line with the increase in temperature from 75°C to 200°C, according to the report by Alkathy et al. This is due to the formation of the acceptor-donor defect complex where the bouncing electrons are attracted to the vicinity of the defects [99]. Unlike many reports, BST films accumulated on Pt/Ti/SiO_2/Si target through RF magnetron sputtering has been resulted in almost the same dielectric constant value at varied temperatures illustrating the most homogeneous film as well as the nonappearance of interfacial barriers inside the film, as have been explored by Yan et al. [124].

From the previous works, it is possible to summarize the mechanisms of how unidopants and codopants affect the performance of a BST as a capacitor. One thing for sure is that substitution of the *A*- and *B*-sites of BST dielectric material by the metals is the main cause for the changes in the dielectric property and capacitive application. For instance, the dielectric constant was enhanced due to an increase in the polarization as the result of the formation of oxygen vacancies, generation of free electrons as well as inner electric potential, and formation of conduction state at the grain edges. The defect dipoles' defect clusters, electrons, and holes are accumulated in a specified region producing elevated dielectric permittivity. The dielectric constant reaches its maximum value at a specific amount of the dopant. It increases up to a specific temperature where it started falling called the Curie temperature.

Dopants also neutralize bouncing electrons found at the crystal as a result of the substitution of *B-site* of BST. The electrons are also trapped by the replaced Ti^{4+} ions. These ultimately resulted in lowering the dielectric loss and the leakage current density. The oxygen vacancies formed after substitution can act as donors of the perovskite structure which produces conduction electrons that are attached to Ti^{4+} and reduced to Ti^{3+}. Then, electrons are surrounded by the completely ionized oxygen vacancies which produce enlarged electron defect-dipole. This ultimately lowers the dielectric loss [99].

It has also been clear that an optimized amount of the dopant mixed with BST increases the rate of polarization of BST and this results in higher energy and enhanced power densities of the BST capacitor where these parameters are usually used as additional criteria for the study of capacitive properties of the BST [125–127]. All these improvements become significant when BST is codoped with more than one element. This is the result of the existence of both acceptor and donor dopants at the codopant material. Holes and electrons are balanced, and therefore, simultaneous improvement in both dielectric constant and dielectric loss is observed. Therefore, codoping BST nanomaterial is a preferable means of synthesizing a BST capacitor with improved energy storing capacity performance [128].

Thus, codoping is often taken as a better doping method as compared to unidoping where more polarization, higher vacancies as well as defects and immobilization of extra electrons were obtained. The codopants substitute *A*- and/or *B*-site components of BST at a time, and hence, more changes or improvements in properties are observed.

The dielectric constants as well as the dielectric loss values of BST samples obtained after addition of the codopants to the BST material, at optimized calcination and sintering temperature, are summarized in Table 1. Values of a few unidoped BST nanomaterials are also included just for comparison purposes. The dielectric properties of doped BST materials, in general, are affected by the calcination and sintering temperature. This is due to the fact that these temperature values do have their own impact on the microstructural arrangement and growth rate of the doped BST crystals. Therefore, it affects the grain size which possesses a significant contribution to the dielectric properties of doped BST materials. Hence, studying and considering the calcination and sintering temperatures are by far very crucial [19].

Looking at Table 1, it is clearly understood that there is a tremendous enhancement in the capacitive nature of almost all doped BST nanomaterials. The dielectric constant values of doped BST have been found much higher than those of pure BST nanomaterial. The dielectric loss has also been lowered more. On the other hand, more improvements in dielectric properties have been observed when BST was codoped with multielements than unidoped with single elements or ions [128]. For instance, La_2O_3/Sb_2O_3 codoped BST has shown a higher dielectric constant than Sb_2O_3-doped BST. Dielectric loss has also been found very small for La_2O_3/Sb_2O_3 codoped BST relative to that of Sb_2O_3 unidoped BST. Such trends are clearly observed in other unidoped and codoped BST. Therefore, it is worthy to conclude that multielement doped BTSs are better capacitors relative to the unidoped BST ones [19, 75, 129]. However, there is also a possibility where codopants might reduce the dielectric properties of BST due to a variety of reasons. (Fe, F)-codoped BSTs have shown smaller dielectric constant along with elevated dielectric loss than the Fe-doped BST and pure BST which means that codoping did not improve the dielectric parameters of the unidoped and pure BST. This is of course due to the fact that the Fe dopant added on the Ti site caused distortion of the perovskite framework [78, 105, 130]. In another observation of Table 1, dielectric properties of the doped BST are affected by variation of sintering and calcination temperatures due to their effect on the number of oxygen vacancies and space charge polarization of the doped BST where increase in sintering temperature mostly resulted in enhanced dielectric constant. Varied relationship of the dielectric loss and sintering temperature has also been observed [73, 78]. Calcination temperatures have the capacity to alter particle size of doped BST which further affect the dielectric properties of the doped BST nanomaterial [73]. Saeed et al. reported lowering of dielectric constant as well as elevation of dielectric loss of Fe-doped BST as a result of increment in calcination temperature [78].

On the other hand, lowered leakage current value of capacitors is an important characteristic of an improved efficiency of the material as well as its respective electric charge accumulating capacity [131]. Table 2 explores the change related to the leakage current of BST as the result of

Table 1: Maximum dielectric constant as well as minimum dielectric loss values of unidoped and codoped BST nanomaterials with their respective optimized calcination and sintering temperature.

Doped BST materials	Maximum dielectric constants	Minimum dielectric losses	Optimized calcination temperatures (°C)	Optimized sintering temperatures (°C)	References
(La, Sb) codoped BST ceramics	8,000	0.0028	1,080	1,290	[19]
La-Mn-Al codoped BST	1,200	0.03	750	900	[55]
Sb_2O_3 doped nonstoichiometric BST ceramics	2,200	0.008	800	1,080	[75]
Zr-doped BST ceramics	—	0.0166	1,100	1,400	[129]
Fe doped BST	1,453.69	0.0063	800	1,200	[78]
Mg^{2+}/K^{+} codoped BST films	479	0.016	500	800	[97]
(Ce, Mn) codoped BST	405	0.075	580	580	[98]
Bi and Li codoped BST	147.752	0.012	1,100	1,450	[99]
$Ba(Mg_{1/3}Nb_{2/3}O_3)$ codoped BST	615	0.03	700	650	[102]
Mg/Nb codoped BST ceramics	336	0.03	700	700	[103]
Fe, F codoped BST	398	0.09	700	800	[105]
La and Co codoped BST films	630	0.025	450	450	[109]
Bi_3NbZrO_9 doped BST ceramics	2,325	0.0048	—	1,280	[110]
Mn/Y codoped BST thin films	855	0.032	700	—	[111]
B_2O_3/CuO codoped BST	1,048	0.0090	950	1,100	[115]
Fe, Co, Ni, Cu, F codoped BST	680	0.001	900	1,200	[116]
PbO-SiO_2-B_2O_3 glass codoped BST	2982	0.004	—	900	[119]
Mg-Mn codoped BST/$MgAl_2O_4$	625	0.0012	1300	1,500	[120]
Fe, Co codoped BST	>10,000	0.075	—	750	[130]
Pt/BST/NiFe/Cu multilayered capacitor	657	0.0137	800	1,350	[131]
La_2O_3 doped Ti-rich BST ceramics	5,381	0.0125	800	1,080	[132]
$BaSiO_3$ doped BST	1,792	0.01	600	1,280	[133]
Dy_2O_3-doped (Ba, Sr) TiO_3 ceramics	5,245	0.0026	800	1,000	[134]
Y_2O_3 and DyO_3 codoped BST	3,658	0.0093	1,250	1,250	[135]
Mn-doped BST thin films	—	0.014	750	—	[136]
Sb_2O_3 doped BST	3,248	0.009	610	1,080	[137]
Pt-Sb codoped BST	2.2×10^6	0.17	—	—	[138]
$Bi_{0.9}La_{0.1}Fe_{0.95}Mn_{0.05}O_3$ codoped BST	—	2×10^{-6}	600	700	[139]
ZrO_2 and MnO_2 codoped BST/MgO	110	0.001	1,150	1,450	[140]
Mn + Y codoped BST powders	2,850	0.0137	900	1,250	[141]
Ni/Ce codoped BST thin film	298	0.018	1,200	1,450	[142]
Al-W codoped BST thin film	400	0.03	450	1,050	[143]
Mg-W codoped BST thin film	361	0.03	450	1,050	[143]

addition of codopants. As can be observed from the table most unidoping as well as codoping of the BST nanomaterial resulted in a reduced leakage current due to the substitution of the *A*- and/or *B*-sites of the BST perovskite which hindered the formation of free electrons and lowered the number of oxygen vacancies [132].

2. Method

2.1. The Synthesis of Codoped BST Nanomaterial. Different methods have been employed to synthesize codoped BST nanomaterials. These include a conventional solid-state reaction technique [19, 32], hydrothermal [133], and sol-gel techniques [70]. The methods at which materials are prepared have significant effects on the surface morphology as well as microstructure of the sample materials [134].

Some of the synthesis methods and the structural change observed as a result of doping are summarized in Table 3. The optimized amount of dopant and the change on the grain of the doped BST are also included. This is due to the fact that they possess an impact on the dielectric characteristics and capacitive application of BST nanomaterial [109]. As can be observed from Table 3, it is clear that most multielement doping processes of BST are carried out through the solid-state reaction method even though there is a question of labour intensiveness, homogeneity, and purity. On the other hand, sol-gel is known for its easiness, small cost, superb composition management, elevated molecular uniformity, enhanced purity, small processing temperature, complex materials' utility of preparation, crystallization rate of the final product, and smaller polluting extent. It is a simple method for doping and to obtain uniform products. Therefore, the sol-gel method is taken as the suitable technique to be utilized during the synthesis of doped BST samples even though it has a disadvantage of resulting in a porous structure as a result of the removal of organic substance and gases while drying [42, 70, 135–137].

3. Results and Discussion

3.1. Characterization of Codoped BST Nanomaterials. The codoped BSTs are usually characterized using methods including XRD, SEM, EDS, XPS, Raman spectroscopy, TGA, and LCR meter measurements to study its crystal structure, grain size, morphology, elemental composition, response to heating, and dielectric properties which determine its capability to be utilized as a capacitor.

X-ray diffraction (XRD) is utilized to resolve the arrangement of a single crystal, crystal structure, and crystallite size of material. The characteristic XRD patterns of pure BST as well as BST codoped with $Ni_{0.5}Zn_{0.5}Fe_2O_4$ (NZF) where the amount of the NZF codopant has been varied as 0.4, 0.6, and 1.0 mol % was obtained. The pure ferroelectric BST has shown a cubic perovskite arrangement, but the addition of 1.0 mol % NZF has changed its structure to a cubic spinel structure. As the NZF composition was elevated, the intensity peak (311) of the spinel phase went to higher values, but the intensity of the pure BST peak (110) has been lowered in the same ratio. This explores the better distribution of ferrite in the composite having perfect homogeneity [138].

It is known that SEM is used to study the surface appearance, topography, composition and microstructure, homogeneity, necking, grain boundary, grain size, and porosity of samples. For instance, it has been used to approve the formation of $BaO\text{-}SiO_2\text{-}B_2O_3$ glass codoped BST thin film composed of 5 vol %, 10 vol %, and 20 vol % of the dopants. A uniform structured $BaO\text{-}SiO_2\text{-}B_2O_3$ glass codoped thin film without fracture was synthesized. The grain size has been reduced from 15 μm of the pure BST to less than 1 μm of the codoped BST. It clearly described the effect of the dopants on the microstructural property which is one of the major factors that determine the energy storing capacity of BST nanomaterials [127].

On the other hand, EDS is a technique applied in exploring the composition of a sample. EDS has been used as a verifying method for the formation of $Ni_{0.5}Zn_{0.5}Fe_2O_4$ codoped $Ba_{0.6}Sr_{0.4}TiO_3$. The intense peaks corresponding to the major components of the BST, Ba, Ti, Fe, and Ni have shown higher amount of abundance at the surface of the $Ni_{0.5}Zn_{0.5}Fe_2O_4$ codoped $Ba_{0.6}Sr_{0.4}TiO_3$ material. Therefore, the formation of codoped BST has been experimentally confirmed [138].

AFM is also another technique that has been utilized as a characterizing parameter of codoped BSTs for its 3D image. The surface morphologies of the $Bi_{0.9}La_{0.1}Fe_{0.95}Mn_{0.05}O_3$ doped BST and BST have been used to approve the formation of doped BST and to investigate the effect of the $Bi_{0.9}La_{0.1}Fe_{0.95}Mn_{0.05}O_3$ on the microstructure of BST. Hence, both materials have uniform arrangements with no cracks on their surfaces. The mean grain of the $Bi_{0.9}La_{0.1}Fe_{0.95}Mn_{0.05}O_3$ codoped BST surface was found higher than the BST film [139].

In more detail but similar to EDS, XPS study is usually used to confirm the surface chemical states, defects as well as compositions of samples. It has been used during the synthesis of Bi/Li codoped BST ceramics. The XPS spectrum of the elements, Ba, Sr, Bi, Li, Ti, O, and C, has confirmed that the ceramics was pure. From the spectrum of the codoped BST ceramics, element peaks for Ba, Sr, Bi, Li, Ti, O, and C have been observed, but only peaks for Ba, Sr, Ti, O, and C were explored at the XPS spectrum of the pure BST. This is an evidence for the effective addition of Bi and Li to BST. The binding energies, 778.19 and 793.14 eV, correspond to the Ba $3d_{5/2}$ and Ba $3d_{3/2}$, while 133.28 and 131.31 eV are the respective binding energies for Sr $3d_{3/2}$, and 131.59 and 131.63 belong to Sr $3d_{5/2}$. The Ti^{4+} $2p_{3/2}$ and Ti^{4+} $2p_{1/2}$ have respective binding energy values of 456.64, 456.67 eV at the undoped BST (BST6 : BL0%), and 462.35, 462.67 eV at the 4 mol % (Bi, Li) codoped BST (BST6 : BL4%). The 528.44 eV major peak corresponds to the BST, while 528.28 eV belongs to the peak of (BST6 : BL4%) revealing an oxygen vacancy lattice located at the Ti-O bond. This was not found in the pure BST. On the other hand, the binding energies 157.43 eV and 162.71 eV are the values for the Bi $4f_{7/2}$ as well as Bi $4f_{5/2}$, respectively, referring to Bi^{3+}. Finally, the peak found at 60.06 eV that is identified as Li_2CO_3 expresses the existence of Li^+ ion [99].

Table 2: Minimum leakage current density of codoped BST as well as the most likely driving force for the change to occur.

Codoped BST samples	Minimum leakage current density (A/cm^2)	Change of leakage current of BST	Most probable reasons	References
Mg/La, Mg/Nb codoped BST	1.4×10^{-8}	Decrease	(i) Insulating property of defect dipoles	[48]
$BaMg_{1/3}Nb_{2/3}O_3$ codoped BST	4×10^{-4}	Decrease	(i) Insulating property of defect dipoles (ii) Charge neutrality balancing	[102]
Mn + Y codoped BST	1.0×10^{-3}	Decrease	(i) Replacement of Ti by the acceptor Mn and Y (ii) Reduction of electron density	[111]
$Bi_{0.9}La_{0.1}Fe_{0.95}Mn_{0.05}O_3/Ba_{0.7}Sr_{0.3}Ti_{0.95}Co_{0.05}O_3$	$\sim2\times10^{-6}$	Decrease	(i) Reduction of electron density	[139]
Ni/Ce codoped BST	1.0×10^{-6}	Decrease	(i) Reduction of donor oxygen vacancies by acceptor Ni^{2+} ions	[142]
Ce-doped BST	4.0×10^{-5}	Decrease	(i) Lowering of free electrons (ii) Trapping of electrons	[144]
Mg–Al codoped BST	1.56×10^{-5}	Decrease	(i) Lowering of oxygen vacancies (ii) Balancing of electrons	[145]
Au-doped BST	3.6×10^{-8}	Decrease	(i) Lowered oxygen vacancies	[146]
Dy-doped BST	1.0×10^{-10}	Decrease	(i) Trapping of electrons (ii) Compensation of ionized oxygen vacancies	[147]
Fe-doped BST	3.0×10^{-9}	Decrease	(i) Lowering of free electrons (ii) Trapping of electrons	[148]

Table 3: Methods used to synthesise doped BST nanomaterial, the optimized amount of the dopant, and structural changes of the grain observed.

Dopants used with BST	Synthesis methods	Optimized amount of dopant (mol %)	Change in grain nature	References
(La, Sb) codoped BST ceramics	Solid state route	0.8 mol % La_2O_3, 0.4 mol % Sb_2O_3	Lowering of average grain size	[19]
Mg/La, Mg/Nb codoped BST thin film	Metalloorganic deposition method	15 mol % (Mg, La, Nb)	No change	[48]
La-Mn-Al codoped BST	Sol-gel method	1 mol % La, 2 mol % Mn, and 1 mol % Al	Enhancement in thickness, uniformity, and compactness of polycrystalline	[55]
Bi-doped BST powders	Sol-gel method	4 mol%	Lowering of crystallite size, the appearance of secondary phases ($BaCO_3$, TiO_2 Bi_2O_3)	[69]
$Mg^{2+/}K^+$ codoped BST films	Sol-gel method	5 mol % Mg^{2+}, 7 mol % K^+	Distortion of lattice, lowering in grain size	[97]
(Ce, Mn) codoped BST thin film	Chemical solution deposition	0.3 M (Ce, Mn)	Slight lattice expansion, gradual grain size reduction	[98]
Bi and Li codoped BST ceramics	Conventional solid-state reaction method	4 mol % (Bi, Li)	Lowering of lattice parameters as well as in-unit cell volume	[99]
(Al, Nb) codoped BST ceramics	Standard solid state ceramic route	1 mol % (Al, Nb)	No apparent change	[100]
$Ba(Mg_{1/3}Nb_{2/3}O_3)$ doped BST thin film	Radiofrequency (RF) magnetron sputtering	4 mol % (Ba, Mg, Nb)	Lowering of film surface roughness, reduction of grain sizes	[102]
Mg/Nb codoped BST ceramics	Solid-state reaction	4 mol. % (Mg, Nb)	Reduction in grain sizes	[103]
Fe and F codoped BST thin films	Modified sol-gel process, RF sputtering	2.4 wt % Fe, 1.8 wt % F	Small reduction of grain size	[105]
(Mn,Y) codoped BST	Modified sol-gel	0.5 mol % Mn, 1.0 mol % Y	Enhancement in lattice parameters and average grain sizes	[106]
La and Co codoped BST films	Metalorganic solution deposition technique	0.25 mol % La, 0.25 mol % Co	Enhancement in uniformity and crystallinity of grains	[109]
$50PbO:30B_2O_3:20SiO_2$-Ag codoped BST	Solid-state ceramic route	8 wt % $50PbO:30B_2O_3:20SiO_2$, 14 vol % Ag	Reduction of interparticle distance of Ag particles	[112]
Sb, Mn codoped BST ceramics	Conventional mixed oxide process	0.03 mol % Sb, 0.08 mol% Mn	Formation of acceptor defects by Mn	[113]
Co-F codoped BST thick-films	Modified sol-gel process	11.8 mol % Co, 35. 4 mol % F	Increment in grain size, formation of a secondary phase	[114]
B_2O_3/CuO codoped BST	Solid-state reaction method	3.0 mol % B_2O_3, and 2.0 mol % CuO,	Increment of the bulk density and grain size, decrease in porous microstructure	[115]
Fe, Co, Ni, Cu, F codoped BST	Sol-gel route	0.09 mol % F, 0.01 mol % (Fe, Co, Ni, Cu)	Increase in crystallite sizes	[116]
(Co, Mn) codoped BST	Traditional ceramic processing	10 mol % (Co, Mn)	Lowering of grain size	[117]
$MgMoO_4$ codoped BST	Solid-state reaction	20 wt % $MgMoO_4$	Change in lattice constant	[118]
PbO-SiO_2-B_2O_3 glass codoped BST	Conventional solid-state routes	10 wt % of glass	Smaller lattice parameters	[119]
Mg–Mn codoped BST/$MgAl_2O_4$	Conventional solid-state reaction	1.0 wt % MgO, 2 wt % $MnCO_3$	Expansion of $MgAl_2O_4$ crystals, elevation of grain size	[120]
$BaAl_2Si_2O_8$ codoped BST glass	Solid state reaction	12 mol Al_2O_3, 22 mol SiO_2, 2 mol BaF_2, 0.1 mol MnO_2	Alteration of crystalline grains from elongated arrangement to cubic, elevation of grain size	[123]
Mn and Y codoped BST	Citrate-nitrate combustion derived powder	0.5 mol % Mn, 1.0 mol % Y	Increment of crystallinity as well as grain size	[124]
BaO-SiO_2-B_2O_3 codoped BST	Conventional solid-state method	20.3 wt % SiO_2, 26.7 wt % B_2O_3	Reduction of porosity, grain size, and pore size	[127]
Fe-Co codoped BST	Modified sol-gel technique	10 mol % (Fe, Co)	Elevation of lattice parameters, lowering crystallite sizes	[130]
Y_2O_3 and DyO_3 codoped BST	Conventional mixed oxide	1 mol % Y_2O_3 and 1 mol % DyO_3	Increment in lattice parameter and grain sizes	[135]

Table 3: Continued.

Dopants used with BST	Synthesis methods	Optimized amount of dopant (mol %)	Change in grain nature	References
Pt-Sb codoped BST	Conventional mixed oxide process	0.15 mol % Sb, 3 mol% SiO_2	Formation of the Schottky barrier	[138]
$Bi_{0.9}La_{0.1}Fe_{0.95}Mn_{0.05}O_3$ codoped BST thin film	Sol-gel method	10 mol% (Bi, La, Fe, Mn)	Increase in average grain size	[139]
ZrO_2 and MnO_2 codoped BST	Solid reaction method	1 wt % Mn, 1.5 wt % Zr	Increase in temperature stability as well as crystal cell parameter	[140]
Mn + Y codoped BST	Conventional electronic ceramic process	0.75 mol% Mn, 0.6 mol% Y	Improvement of the crystallization	[141]
Ni/Ce codoped BST thin film	Conventional mixed oxide method, and pulsed laser deposition	1 mol % Ni, 1 mol % Ce	Enhanced crystallinity, less rough surface, and reduction of particle size	[142]
Al-W codoped BST	Pulsed laser deposition	3 wt % Al, 2 wt % W	Slight increase in lattice parameter, reduction of grain size, and change in shape from polygonal grains to an elongated shape	[143]
Mg-W codoped BST	Pulsed laser deposition	5 wt % Mg, 2 wt % W	Slight increase in lattice parameter, elevation of grain size, and change in shape from polygonal grains to rounded shape	[143]
Fe_2O_3 doped BST	Chemical solution deposition with spin coating technique	15 mol%	Increase in crystallinity and change in orientation	[149]
Y^{3+}/Mn^{2+} codoped BST thin films	Conventional solid-state	0.7 mol % Y^{3+}, 0.1 mol % Mn^{2+}	Lowering of grain size	[150]
Al_2O_3-MgO codoped BST	Traditional electrical ceramic methods	20 wt % (Al, Mg)	A phase change from BST to $BaAl_{12}O_{19}$	[151]
$Ni_{0.5}Zn_{0.5}Fe_2O_4$ codoped BST	Standard solid state reaction route	0.4 mol $Ni_{0.5}Zn_{0.5}Fe_2O_4$	Phase change from cubic perovskite structure to the cubic spinel structure	[152]
Al_2O_3-SiO_2-AlF_3-MnO_2 codoped BST glass	Solid-state reaction route	4 mol% AlF_3, 1 mol % MnO_2	Change of grain morphology to a more uniform arrangement	[153]
Zn-B-Si-O codoped BST	Sol-gel process	10 mol % Zn-B-Si-O	Reduction of grain size	[154]
$Ni_{0.8}Co_{0.2}Fe_2O_4$ codoped BST	Solid-state reaction method	20 mol % $Ni_{0.8}Co_{0.2}Fe_2O_4$	Elevation of in lattice constant and grain size	[155]
Fe, Ni codoped BST	Sol-gel technique	10 mol % (Fe, Ni)	Reduction in average crystallite size and increasing of lattice parameter	[159]
(Zn, Tb) codoped BST	Sol-gel process	1 wt. % (Zn, Tb)	Small lattice expansion	[160]
Y_2O_3, Nb_2O_5 codoped BST	Solid-phase method	0.3 mol % (Y, Nb)	No change	[161]

Reports have usually been using Raman spectroscopy as a very sensitive spectroscopic method that is utilized to obtain the structural data. It has been used as a confirmatory technique for the formation of (Al, Nb) codoped BST. A peak at 150 cm^{-1} which belongs to the movement of Ba^{2+} and Sr^{2+} ions that is responsive to the *A*-site replacement (ETO mode) has been observed. Another peak at ~237 cm^{-1} peak which corresponds to A1 (TO) part of the cubic F1u soft mode was also obtained. On the other hand, a peak observed at 500–700 cm^{-1} is the result of oxygen octahedron TiO_6 stretching mode (A1g (O)), while the ~760 cm^{-1} represents the movement of Ti along with oxygen (A1g and Eg mode), that is related to the altering of the Ti-O-Ti bond angle. It also shows the replacement of Ti^{4+} by $(Al_{0.5}Nb_{0.5})^{4+}$ [100].

Thermal gravimetric (TG) analysis is another technique of characterization that is employed for the thermal investigation which determines weight variation of a sample due to temperature as well as time change, in a managed surrounding. It has been used as an identifier of the precursors and reaction types during the synthesis of Fe, Co, Ni, Cu, and F codoped BST. TG curves of BST and Fe, Co, Ni, Cu, F codoped BST starting materials which are heated at a maximum temperature of 1,200°C were observed at the spectrum. Three possible reductions of sample weights were obtained. The peaks belong to the barium-titanium acetate as well as BST gel precursors. The first one corresponds to the evaporation of water as well as acetic acid found at the starting materials as a result of spray drying. This occurs at the range of 100°C–220°C and explored a weight loss of 6–8%. The other one is the one which appeared at 250 to 400°C and represented a weight loss of 36–45%. This step explored and then changed the metallorganic precursor into metastable oxycarbonate. The last step occurred at the range of 550°C to 650°C having a weight loss of 9–12%. It represented the decomposition of metastable oxycarbonate to BST crystal. The second stage expressed that weight loss of Cu-F codoped BST is smaller as compared to that of BST precursors. On the other hand, the remaining codoped BST had larger weight losses than BST precursors. At the third stage, the decomposition for the Fe-F codoped as well as Cu-F codoped raw materials occurred at smaller temperatures relative to the pure BST precursor [116].

Finally, the collective impacts of the codopants over the dielectric characteristics of BST nanomaterial are investigated by using an LCR meter. It is used to determine dissipation factor *D* or quality factor *Q* and capacitance which are helpful to determine the dielectric constant as well as dielectric loss specimen understudy [70, 140–142]. These properties are crucial preconditions for the codoped BST nanomaterial to be utilized as a capacitor of different energy-storing materials. The dielectric constant is highly affected by thermal motion as well as thermal expansion of BST sample. In general, the dielectric constant value increases when the sintering temperature is lowered, while for the dielectric loss, it is almost a reverse phenomenon. Such a result was obtained when BST was codoped with Bi and Li. The codoped samples have been resulted in enhanced dielectric permittivity possessing a dielectric loss of less than 0.1 in the temperature range of 75°C–200°C, but at a temperature higher than 200°C, the materials result in higher dielectric loss [99].

The impact of codopants over the dielectric property of BST can be expressed through the determination of the leakage current (LC) of BST and the codoped BST nanomaterial where lower LC is the goal to be achieved. For instance, Alema and Pokhodnya used LC versus voltage graphs to examine the leakage current and studied the impact of the $BaMg_{1/3}Nb_{2/3}O_3$ over the leakage current of BST. The leakage current of Mg/Nb codoped BST film was found smaller as compared to the BST film, where Mg/Nb codoping confirmed that the charge neutrality balancing lowers leakage current of the BST film [102].

3.2. BST Nanomaterial as a Capacitor. BST nanomaterial is a known perovskite nanomaterial with an elevated dielectric constant, smaller dielectric constant, and lower leakage current density. It is being broadly studied in search of its application as a capacitor because of its improved energy accumulation capacity as well as performance. BST nanomaterial possesses favourable ferroelectric as well as dielectric premises including polarizability, piezoelectricity, pyroelectricity, and electro-optic activity which make it a perfect energy-storing material with a minimum refreshing time or charging time of 1–10 seconds [143–146]. BST is conveniently applied in the preparation of energy-storing electronic devices such as capacitors, dynamic random access memories (DRAM), magnetic core memory (MCM), monolithic microwave integrated circuit (MMIC), piezoelectric sensors, voltage-controlled oscillators, microwave state changers, and tunable filter. When BST ceramics, with Sr content ≤ 0.4 and Curie temperature lower than room temperature, it is taken as the encouraging capacitor material of fluctuating potential electronics. This is because of the necessary ferroelectric along with dielectric properties it possesses [32, 42, 147–149, 156–158]. It is then on the verge of completely replacing the conventional dielectric materials such as Ta_2O_5 and SiO_2. It is also a crucial component during the preparation of fixed capacitors acting as a charge-accumulator where no space is needed at the outer part of printed-circuit-board (PCB) [156]. BST is a preferable nominee of post-1 Gbit DRAM capacitors. BST multilayered capacitor must fulfil the requirements where it must possess upper as well as lower electrodes. The electrodes must possess high metallic conductivity; they should be chemically inert toward oxidation, having appreciable adhesion as well as flat interfacial rows that result in enhanced capacitance along with small current leakage [105]. Adding BST within a DRAM cell has been found as largely needed since the small leakage current assures the electronic charge data accumulated during DRAM functioning [78]. However, electrode material of BST thin films must be selected carefully so as to block the occurrence of a small dielectric interfacial row. For such an objective, electrodes of expensive metals including platinum (Pt), ruthenium (Ru), and iridium (Ir) have been normally used. This definitely tells that the electrical passage techniques are highly

impacted by the interfacial region located between BST and the electrode [150]. It is now clear that BST nanomaterial has been widely used as a capacitor material.

On the other hand, it is already reported and clarified that both unidoping and codoping have been observed enhancing the dielectric properties of BST capacitors. This is done through enhancement in the number of holes and electrons which results in highly polarized samples, and hence, higher dielectric constant as well as higher capacitance is obtained. Meanwhile, the number of oxygen vacancies is lowered through the formation of a defect-dipole complex with the dopants which results in the reduction of dielectric loss. Electrons are also trapped by the dopant ions causing the leakage current to get reduced. These improved properties ultimately result in enhanced capacitive applications of BST. The effect of dopants on the energy storing capacity of BST are mainly expressed through energy density, efficiency, electrical breakdown strength, and power density of the doped BST capacitor [125–127].

For instance, pure $Ba_{0.4}Sr_{0.6}TiO_3$ nanopowders have been produced through a sol-gel method at 750°C which resulted in electrical breakdown strength of ~240 kV/cm, and energy storage density ~1.23 J/cm^3 has been reported [151]. A study by Xie et al. has also explored that doping of BST with Fe via the sol-gel deposition method resulted in an enhanced polarization which led to a higher discharged energy density equal to 7.6 J/cm^3 [152]. Diao et al. reported that a SiO_2 dopant added to BST ($Ba_{0.4}Sr_{0.6}TiO_3$) ceramics through the traditional solid-state reaction method resulted in improved breakdown strength of 134 kV/cm and increased energy density of 0.86 J/cm^3, due to the increase in the amount of oxygen vacancies [153]. It has also been explored that creating a heterostructure system with BST forms an interfacial layer which has visible impacts over the dielectric parameters, breakdown strength, power density, and energy accumulating capacity of the thin films. A heterostructure composite of $BaSn_{0.15}Ti_{0.85}O_3/Ba_{0.6}Sr_{0.4}TiO_3$ encompassing a 4 mm thickness as well as about 30 mm diameter was gained via traditional ceramic processing. It possessed an energy storage density of 43.28 J/cm^3 and a bias electric field of 2.37 MV/cm possessing an enhanced power density of 6.47 MW/cm^3. An increased dielectric constant as well as lowered loss tangent was also resulted [154]. Likewise, elevated dielectric constant, breakdown strength, and energy density were explored when polyimide/sub-10 nm $Ba_{0.7}Sr_{0.3}TiO_3$ nanocomposites were prepared via an in situ polymerization technique in which BST has been blended with 1,3-bis(4-aminophenoxy)benzene (BAPB) and pyromellitic dianhydride (PMDA) monomers prior to spin casting along with thermal imidization [155]. Many other reports confirmed that the addition of an optimized amount of dopant or formation of a heterostructure composite resulted in enhanced capacitive parameters (energy density and power density) of the BST capacitive material [125–127].

It is now inferred that codoping of BST has an effect on the energy storing capacity of BST. Such an impact has been observed when BST was codoped with $BaO\text{-}SiO_2\text{-}B_2O_3$ containing glass. The addition of the dopants has resulted in an elevation of breakdown strength from 12.1 kV/mm of pure BST to 23.9 kV/mm of the doped one. On the other hand, the remnant polarization has also been lowered from 2.7 mC/cm^2 of pure BST to a minimum value of 0.29 mC/cm^2 of codoped BST. These two results were mainly driven by the lowering of grain as well as pore sizes and the reduction of porosity. The enhancement in breakdown strength as well as lowering in remnant polarization of the codoped BST led to an elevated energy density. It has been elevated from 0.37 J/cm^3 to 0.89 J/cm^3 after having been codoped by $BaO\text{-}SiO_2\text{-}B_2O_3$ containing glass [127]. Similarly, a BST glass-ceramics prepared after doping of BST with $BaAl_2Si_2O_8$ has shown enhanced dielectric constant elevated from 119 to 317 and lowered breakdown strength from 56.8 to 36.6 kV/mm at a higher crystallization temperature of 950°C. These parameters led to the achievement of the highest energy density of 3.0 J/cm^3 that is higher as compared to the value for the conventional capacitors. Hence, $BaAl_2Si_2O_8$ codoped BST is selected as an efficient dielectric sample that can be utilized in enhanced energy storage density capacitors [123]. A codoped BST capacitor has shown enhanced energy density and efficiency when BST was codoped with Ce and Mn dopants. (Ce, Mn) codoped BST has been resulted in an energy density (W) of 18.01 J/cm^3 and higher energy storage efficiency (η) of 75.1% under 2,000 kV/cm relative to the BST, Ce, as well as Mn-doped BSTs were recorded. This is even higher than other types of capacitors such as $PbZrO_3$ thin films [98].

Since most of the dielectric properties of unidoped BST have been improved through multielement doping, multielement doped (codoped) BSTs have shown sufficient dielectric properties to be selected as perfect capacitors of different energy-storing materials [98].

Looking at both the unidoped BST and multielement doped (co-doped) BST samples synthesized through a variety of methods, it is possible to point out that the improvements in the dielectric properties and capacitive application are not smooth. That is, addition of the dopants into BST might increase the dielectric constant which can possibly lead to the elevation of the dielectric loss and leakage current density of BST. Only few dopants are able to increase the dielectric properties and capacitance of BST while lowering the dielectric loss and leakage current density of BST. On the other hand, most of the enhancements of the capacitive application of BST following the incorporation of multielement dopants to BST are still at a small scale. Hence, all the points explained previously are taken as limitations of doping BST so as to enhance the capacitive utilization of BST. Thus, we believe that large scale application of the doped BST samples in capacitors is recommended as a future work. Finding the best conditions where increment of capacitance while reducing the dielectric loss and leakage current density of BST as the result of incorporation of multielements is also supposed to be a forthcoming task.

4. Conclusion

From the articles, it is possible to summarize that BST nanomaterial has of its own proved capacitive nature. However, it is one of the possible materials to be utilized

during the fabrication of capacitors. Meanwhile, doping changes the dielectric and physical characteristics of BST nanomaterial where most of the capacitor characteristics of BST are enhanced. The dielectric constant is increased up to a certain optimized amount of the dopant until which cure temperature is reached. Dielectric loss and leakage current density are reduced to a lower value. According to many reports, codoping is in the way of bringing about improved dielectric parameters of BST nanomaterial which helps it to be the right choice for its capacitive application by enhancing its energy storage density and efficiency. However, doping does not always improve the dielectric properties of BST, and there are cases where it results in lowering of the properties. It is also worthy to say that all the single metal dopants which are expected to increase the dielectric parameters as well as capacitive application of BST were already disclosed except for a few. Hence, attention must now be given to the codopants (multielement doping) which can improve the properties of capacitors composed of BST nanomaterial. Therefore, doped BST capacitors are good future candidates to be used.

Data Availability

The datasets used and/or analysed during the current study are available freely online.

Conflicts of Interest

The authors declare that they have no conflicts of interest.

Authors' Contributions

All authors conceptualized and designed the study. Material preparation, data collection, and analysis were performed by Balachandran Ruthramurthy and Kiflom Gebremedhn Kelele. The first draft of the manuscript was written by Balachandran Ruthramurthy, and all authors commented on the previous version of the manuscript. All authors read and approved the final manuscript.

Acknowledgments

The authors acknowledge the backing provided by Adama Science and Technology University, Ethiopia, towards this work.

References

[1] N. Liu, R. Liang, Z. Zhou, and X. Dong, "Designing lead-free bismuth ferrite-based ceramics learning from relaxor ferroelectric behavior for simultaneous high energy density and efficiency under low electric field," *Journal of Materials Chemistry C*, vol. 6, no. 38, pp. 10211–10217, 2018.

[2] S. Tong, B. Ma, M. Narayanan et al., "Lead lanthanum zirconate titanate ceramic thin films for energy storage," *ACS Applied Materials and Interfaces*, vol. 5, no. 4, pp. 1474–1480, 2013.

[3] F. Han, G. Meng, F. Zhou et al., "Dielectric capacitors with three-dimensional nanoscale interdigital electrodes for energy storage," *Science Advances*, vol. 1, no. 9, Article ID e1500605, 2015.

[4] Q. Bao, J. Wu, L. Fan et al., "Electrodeposited NiSe2 on carbon fiber cloth as a flexible electrode for high-performance supercapacitors," *Journal of Energy Chemistry*, vol. 26, no. 6, pp. 1252–1259, 2017.

[5] N. Mohammadian, A. Moshaii, A. Alizadeh, S. Gharibzadeh, and R. Mohammadpour, "Influence of perovskite morphology on slow and fast charge transport and hysteresis in the perovskite solar cells," *The Journal of Physical Chemistry Letters*, vol. 7, no. 22, pp. 4614–4621, 2016.

[6] Y. Wu, Y. Fan, N. Liu et al., "Enhanced energy storage properties in sodium bismuth titanate-based ceramics for dielectric capacitor applications," *Journal of Materials Chemistry C*, vol. 7, no. 21, pp. 6222–6230, 2019.

[7] J. Wei, T. Yang, and H. Wang, "Excellent energy storage and charge-discharge performances in PbHfO3 antiferroelectric ceramics," *Journal of the European Ceramic Society*, vol. 39, no. 2-3, pp. 624–630, 2019.

[8] Q. Yuan, G. Li, F.-Z. Yao et al., "Simultaneously achieved temperature-insensitive high energy density and efficiency in domain engineered $BaTiO_3$-Bi $(Mg_{0.5}Zr_{0.5})$ O_3 lead-free relaxor ferroelectrics," *Nano Energy*, vol. 52, pp. 203–210, 2018.

[9] J. R. Miller and P. Simon, "Electrochemical capacitors for energy management," *Science*, vol. 321, no. 5889, pp. 651-652, 2008.

[10] K. M. Slenes, P. Winsor, T. Scholz, and M. Hudis, "Pulse power capability of high energy density capacitors based on a new dielectric material," *IEEE Transactions on Magnetics*, vol. 37, no. 1, pp. 324–327, 2001.

[11] R. Xu, B. Li, J. Tian et al., "$Pb_{0.94}La_{0.04}$ $[(Zr_{0.70}Sn_{0.30})_{0.90}$ $Ti_{0.10}]$ O_3 antiferroelectric bulk ceramics for pulsed capacitors with high energy and power density," *Applied Physics Letters*, vol. 110, no. 14, Article ID 142904, 2017.

[12] C. W. Ahn, G. Amarsanaa, S. S. Won, S. A. Chae, D. S. Lee, and I. W. Kim, "Antiferroelectric thin-film capacitors with high energy-storage densities, low energy losses, and fast discharge times," *ACS Applied Materials and Interfaces*, vol. 7, no. 48, pp. 26381–26386, 2015.

[13] C. Xu, Z. Liu, X. Chen et al., "Pulse discharge properties of PLZST antiferroelectric ceramics compared with ferroelectric and linear dielectrics," *AIP Advances*, vol. 7, no. 11, Article ID 115108, 2017.

[14] Z. Liu, X. Dong, Y. Liu, F. Cao, and G. Wang, "Electric field tunable thermal stability of energy storage properties of PLZST antiferroelectric ceramics," *Journal of the American Ceramic Society*, vol. 100, no. 6, pp. 2382–2386, 2017.

[15] A. Saeed, B. Ruthramurthy, W. H. Yong et al., "Structural and electrical properties of nickel–iron thin film on copper substrate for dynamic random access memory applications," *Russian Journal of Electrochemistry*, vol. 52, no. 8, pp. 788–795, 2016.

[16] R. Balachandran, H. K. Yow, B. H. Ong, R. Manickam, V. Saaminathan, and K. B. Tan, "Effects of ultrasonic field in pulse electrodeposition of NiFe film on Cu substrate," *Journal of Alloys and Compounds*, vol. 481, no. 1-2, pp. 336–339, 2009.

[17] J. R. Miller and A. Burke, "Electrochemical capacitors: challenges and opportunities for real-world applications," *Electrochemical Society Interface*, vol. 17, no. 1, pp. 53–57, 2008.

[18] Y. Li and Y. Qu, "Dielectric properties and substitution mechanism of samarium-doped Ba0. 68Sr0. 32TiO3 ceramics," *Materials Research Bulletin*, vol. 44, no. 1, pp. 82–85, 2009.

[19] C. Zhang and Y. F. Qu, "Dielectric properties and phase transitions of La2O3-and Sb2O3-doped barium strontium titanate ceramics," *Transactions of Nonferrous Metals Society of China*, vol. 22, no. 11, pp. 2742–2748, 2012.

[20] R. Pohl, R. Gilman, G. A. Miller, and K. Pachucki, "Muonic hydrogen and the proton radius puzzle," *Annual Review of Nuclear and Particle Science*, vol. 63, no. 1, pp. 175–204, 2013.

[21] Z. S Iro, C. Subramani, and S. Dash, "A brief review on electrode materials for supercapacitor," *International Journal of Electrochemical Science*, vol. 11, no. 12, pp. 10628–10643, 2016.

[22] R. A. Sawitri, L. Suryanti, F. U. Zuhri, and M. Diantoro, "Dielectric properties of dirt sugarcane sediment (DSS) extract-$BaTiO_3$ for organic supercapacitors," in *IOP Conference Series: Materials Science and Engineering*,IOP Publishing, Philadelphia, USA, 2019.

[23] A. A. Mustikasari, M. Diantoro, N. Mufti, R. Suryana, and R. Suryana, "The effect of nano ZnO morphology on structure, dielectric constant, and dissipation factor of CA-nano ZnO/ITO films," *Jurnal Neutrino*, vol. 10, no. 2, pp. 65–68, 2018.

[24] M. Z. Masrul, T. Suprayogi, M. Diantoro, A. Fuad, E. Latifah, and A. Hidayat, "The effect of light irradiation on performance of photo-supercapacitor of FTO/TiO2-ZnO-β Carotene-Quercetin/Carbon/Al/PVDF-BaTiO3/Al," in *IOP Conference Series: Materials Science and Engineering*,IOP Publishing, Philadelphia, USA, 2019.

[25] H. S. Nan, X. Y. Hu, and H. W. Tian, "Recent advances in perovskite oxides for anion-intercalation supercapacitor: a review," *Materials Science in Semiconductor Processing*, vol. 94, pp. 35–50, 2019.

[26] R. Jacob, H. G. Nair, and J. Isac, "Impedance spectroscopy and dielectric studies of nanocrystalline iron doped barium strontium titanate ceramics," *Processing and Application of Ceramics*, vol. 9, no. 2, pp. 73–79, 2015.

[27] C. Xu, Z. Liu, X. Chen et al., "High charge-discharge performance of $Pb_{0.98}La_{0.02}$ $(Zr_{0.35}Sn_{0.55}Ti_{0.10})_{0.995}$ O_3 antiferroelectric ceramics," *Journal of Applied Physics*, vol. 120, no. 7, Article ID 074107, 2016.

[28] M. S. Alkathy and K. James Raju, "Enhancement of dielectric properties and energy storage density of bismuth and lithium co-substituted strontium titanate ceramics," *Ceramics International*, vol. 44, no. 9, pp. 10367–10375, 2018.

[29] A. Burke, "Ultracapacitors: why, how, and where is the technology," *Journal of Power Sources*, vol. 91, no. 1, pp. 37–50, 2000.

[30] A. Chu and P. Braatz, "Comparison of commercial supercapacitors and high-power lithium-ion batteries for power-assist applications in hybrid electric vehicles: I. Initial characterization," *Journal of Power Sources*, vol. 112, no. 1, pp. 236–246, 2002.

[31] A. G. Pandolfo and A. F. Hollenkamp, "Carbon properties and their role in supercapacitors," *Journal of Power Sources*, vol. 157, no. 1, pp. 11–27, 2006.

[32] Y. Fan, Z. Zhou, Y. Chen, W. Huang, X. Dong, and X. Dong, "A novel lead-free and high-performance barium strontium titanate-based thin film capacitor with ultrahigh energy storage density and giant power density," *Journal of Materials Chemistry C*, vol. 8, no. 1, pp. 50–57, 2020.

[33] T. Mikolajick, S. Slesazeck, M. H. Park, and U. Schroeder, "Ferroelectric hafnium oxide for ferroelectric random-access memories and ferroelectric field-effect transistors," *MRS Bulletin*, vol. 43, no. 5, pp. 340–346, 2018.

[34] S. M. Rhim, S. Hong, H. Bak, and K. Kim, "Effects of B_2O_3 addition on the dielectric and ferroelectric properties of $Ba_{0.7}Sr_{0.3}TiO_3$ ceramics," *Journal of the American Ceramic Society*, vol. 83, no. 5, pp. 1145–1148, 2004.

[35] R. Pinjari, N. Burange, and B. Aldar, "Structural and electrical analysis of strontium substituted barium titanate," *International Journal of Engineering Research and Technology*, vol. 3, pp. 209–213, 2014.

[36] T. M. Shaw, Z. Suo, M. Huang, E. Liniger, R. B. Laibowitz, and J. D. Baniecki, "The effect of stress on the dielectric properties of barium strontium titanate thin films," *Applied Physics Letters*, vol. 75, no. 14, pp. 2129–2131, 1999.

[37] A. Kostopoulou, K. Brintakis, N. K. Nasikas, and E. Stratakis, "Perovskite nanocrystals for energy conversion and storage," *Nanophotonics*, vol. 8, no. 10, pp. 1607–1640, 2019.

[38] A. Ahmed, I. A. Goldthorpe, and A. K. Khandani, "Electrically tunable materials for microwave applications," *Applied Physics Reviews*, vol. 2, no. 1, Article ID 011302, 2015.

[39] R. York, J. Speck, T. Taylor et al., "BaSrTiO/sub 3/interdigitated capacitors for distributed phase shifter applications," *IEEE Microwave and Guided Wave Letters*, vol. 10, no. 11, pp. 448–450, 2000.

[40] S. E. Moon, H. C. Ryu, M. H. Kwak, Y. T. Kim, S. J. Lee, and K.-Y. Kang, "X-Band phased array antenna using ferroelectric (Ba, Sr) TiO_3 coplanar waveguide phase shifter," *ETRI Journal*, vol. 27, no. 6, pp. 677–684, 2005.

[41] R. Balachandran, H. K. Yow, R. M. Manickam, and V. Saaminathan, "Simulated dielectric characteristics of Pt/BST/Ni-Fe/Cu multilayer capacitor stack for storage application," in *Proceedings of the 2006 IEEE International Conference on Semiconductor Electronics*, IEEE, Kuala Lumpur, Malaysia, October 2006.

[42] R. Balachandran, H. K. Yow, B. H. Ong et al., "Phase formation and dielectric properties of $Ba_{0.5}$ $Sr_{0.5}$ TiO_3 by slow injection sol–gel technique," *Journal of Materials Science*, vol. 46, no. 6, pp. 1806–1813, 2011.

[43] J. D. Baniecki, T. Shioga, and K. Kurihara, "Barium strontium titanate thin film capacitors for low inductance decoupling applications," *MRS Proceedings*, vol. 748, no. 1, pp. U151–10, 2002.

[44] A. Tombak, J. P. Maria, F. Ayguavives et al., "Tunable barium strontium titanate thin film capacitors for RF and microwave applications," *IEEE Microwave and Wireless Components Letters*, vol. 12, no. 1, pp. 3–5, 2002.

[45] A. Kumari and B. Dasgupta Ghosh, "Effect of strontium doping on structural and dielectric behaviour of barium titanate nanoceramics," *Advances in Applied Ceramics*, vol. 117, no. 7, pp. 427–435, 2018.

[46] P. R. Arya, P. Jha, and A. K. Ganguli, "Synthesis, characterization and dielectric properties of nanometer-sized barium strontium titanates prepared by the polymeric citrate precursor method," *Journal of Materials Chemistry*, vol. 13, no. 2, pp. 415–423, 2003.

[47] L. Zhang, J. Zhai, and X. Yao, "Dielectric properties of barium strontium titanate thick films prepared by electrophoretic deposition," *Materials Research Bulletin*, vol. 44, no. 5, pp. 1058–1061, 2009.

[48] S.-Y. Chen, H.-W. Wang, and L.-C. Huang, "Electrical properties of Mg/La, Mg/Nb co-doped $(Ba_{0.7}Sr_{0.3})$ TiO_3 thin films prepared by metallo-organic deposition method," *Japanese Journal of Applied Physics*, vol. 40, no. 8R, p. 4974, 2001.

[49] Z. Xu, D. Yan, D. Xiao, P. Yu, and J. Zhu, "Dielectric enhancement of $BaSrTi_{1.1}O_3/BaSrTi_{1.05}O_3/BaSrTiO_3$ multilayer thin films prepared by RF magnetron sputtering," *Ceramics International*, vol. 39, no. 2, pp. 1639–1643, 2013.

[50] D. Berlincourt, "Piezoelectric ceramic compositional development," *Journal of the Acoustical Society of America*, vol. 91, no. 5, pp. 3034–3040, 1992.

[51] F. Zimmermann, M. Voigts, W. Menesklou, and E. Ivers-Tiffée, "$Ba_{0.6}Sr_{0.4}TiO_3$ and $BaZr_{0.3}Ti_{0.7}O_3$ thick films as tunable microwave dielectrics," *Journal of the European Ceramic Society*, vol. 24, no. 6, pp. 1729–1733, 2004.

[52] A. Tkach and P. M. Vilarinho, "Materiales de titanato de estroncio dopados con escandio: estructura, microestructura y propiedades dielectricas," *Boletin de la Sociedad Espanola de Ceramica y Vidrio*, vol. 47, no. 4, pp. 238–241, 2008.

[53] G. Singh Kathait, V. Rohilla, P. Thapliyal, D. Biswas, and S. Singh, "Effect of different strontium content on dielectric properties of barium strontium titanate ceramic," *Int. J. Latest Technol. Eng. Manage. Appl. Sci*, vol. 6, p. 75, 2017.

[54] S. K. Godara, V. Kaur, K. Chuchra et al., "Impact of Zn^{2+}-Zr^{4+} substitution on M-type Barium Strontium Hexaferrite's structural, surface morphology, dielectric and magnetic properties," *Results in Physics*, vol. 22, Article ID 103892, 2021.

[55] M.-Y. Fan and S.-L. Jiang, "Influence of La-Mn-Al Co-doping on dielectric properties and structure of BST Thick film," *Journal of Electronic Science and Technology*, vol. 7, no. 3, pp. 281–285, 2009.

[56] T. Itoh, S. T. Shinjiro Tashiro, and H. I. Hideji Igarashi, "Fabrication of multilayer barrier layer capacitors with semiconducting (Ba, Sr) TiO3 ceramics," *Japanese Journal of Applied Physics*, vol. 32, no. 9S, p. 4261, 1993.

[57] K. G. Kelele, A. Tadesse, T. Desalegn, S. Ghotekar, R. Balachandran, and H. C. A. Murthy, "Synthesis and characterizations of metal ions doped barium strontium titanate (BST) nanomaterials for photocatalytic and electrical applications: a mini review," *International Journal of Materials Research*, vol. 112, no. 8, pp. 665–677, 2021.

[58] A. Nemudry, E. L. Goldberg, M. Aguirre, and M. Á. Alario-Franco, "Electrochemical topotactic oxidation of non-stoichiometric perovskites at ambient temperature," *Solid State Sciences*, vol. 4, no. 5, pp. 677–690, 2002.

[59] M. Jain, S. B. Majumder, R. S. Katiyar, F. A. Miranda, and F. W. Van Keuls, "Improvement in electrical characteristics of graded manganese doped barium strontium titanate thin films," *Applied Physics Letters*, vol. 82, no. 12, pp. 1911–1913, 2003.

[60] S. Y. Lee and T.-Y. Tseng, "Electrical and dielectric behavior of MgO doped $Ba_{0.7}Sr_{0.3}TiO_3$ thin films on Al_2O_3 substrate," *Applied Physics Letters*, vol. 80, no. 10, pp. 1797–1799, 2002.

[61] S. Y. Wang, B. L. Cheng, C. Wang et al., "Raman spectroscopy studies of Ce-doping effects on $Ba_{0.5}Sr_{0.5}TiO_3$ thin films," *Journal of Applied Physics*, vol. 99, no. 1, Article ID 013504, 2006.

[62] S Z. Wang, J. X. Liao, H. Y. Yang, J. Q. Huang, W. F. Zhang, and M. Q. Wu, "Preparation and dielectric properties of Ce-doped barium strontium titanate nano-powders," *Integrated Ferroelectrics*, vol. 163, no. 1, pp. 116–123, 2015.

[63] N. Kevin, C. Borderon, S. Pavy, and W. Hartmut, "Gundel. Realization and characterization of manganese doped BST thin films for reflectarray applications," in *Proceedings of the 2013 Joint IEEE International Symposium on Applications of Ferroelectric and Workshop on Piezoresponse Force Microscopy (ISAF/PFM)*, IEEE, Prague, Czech Republic, July 2013.

[64] J. Li, F. Li, C. Li, G. Yang, Z. Xu, and S. Zhang, "Evidences of grain boundary capacitance effect on the colossal dielectric permittivity in (Nb+ In) co-doped TiO_2 ceramics," *Scientific Reports*, vol. 5, no. 1, pp. 8295-8296, 2015.

[65] S. Mandal, S. Pal, A. K. Kundu et al., "Direct view at colossal permittivity in donor-acceptor (Nb, In) co-doped rutile TiO 2," *Applied Physics Letters*, vol. 109, no. 9, Article ID 092906, 2016.

[66] Y. Song, X. Wang, Y. Sui et al., "Origin of colossal dielectric permittivity of rutile $Ti_{0.9}In_{0.05}Nb_{0.05}O_2$: single crystal and polycrystalline," *Scientific Reports*, vol. 6, no. 1, pp. 21478–8, 2016.

[67] X.-F. Liang, W.-B. Wu, and Z.-Y. Meng, "Microstructure and dielectric tunable properties of Al_2O_3-doped barium strontium titanate in the paraelectric state," *Chin. J. Inorg. Mater*, vol. 18, no. 6, pp. 1240–1244, 2003.

[68] M. W. Cole, P. C. Joshi, M. H. Ervin, M. C. Wood, and R. L. Pfeffer, "The influence of Mg doping on the materials properties of Ba1− xSrxTiO3 thin films for tunable device applications," *Thin Solid Films*, vol. 374, no. 1, pp. 34–41, 2000.

[69] A. Sadeghzadeh Attar, E. Salehi Sichani, and S. Sharafi, "Structural and dielectric properties of Bi-doped barium strontium titanate nanopowders synthesized by sol–gel method," *Journal of Materials Research and Technology*, vol. 6, no. 2, pp. 108–115, 2017.

[70] V. Eswaramoorthi, S. Sebastian, and R. V. Williams, "Influence of Ga doping on the structural, optical and electrical properties of $Ba_{0.6}Sr_{0.4}TiO_3$ thin films," *International Research Journal of Science and Technology*, vol. 4, pp. 86–91, 2015.

[71] M. Y. Shahid, M. N. Rasheed, K. Fatima et al., "synthesis, characterization and evaluation of ferroelectric and dielectric behavior of Ni-doped $Ba_{0.7}Sr_{0.3}TiO_3$ thin films prepared via sol-gel route," *Digest Journal of Nanomaterials and Biostructures*, vol. 12, no. 4, 2017.

[72] K. Asa Deepthi, R. Balachandran, B. H. Ong et al., "Phase formation and surface morphology of nickel doped $Ba_{1-x}Sr_xTiO_3$ ceramics prepared by sol–gel technique," *Materials Research Innovations*, vol. 18, 2014.

[73] A. D. Kakumani, B. Ruthramurthy, H. Y. Wong, B. H. Ong, K. B. Tan, and H. K. Yow, "Microstructure and dielectric properties of nickel-doped $Ba_{0.7}Sr_{0.3}TiO_3$ ceramics fabricated by solgel method," *International Journal of Applied Ceramic Technology*, vol. 13, no. 1, pp. 177–184, 2016.

[74] I. Novianty, K. Seminar, and I. Budiastra, "Electrical photoconductivity of Ta2O5 doped based on $Ba_{0.5}S_{0.5}TiO_3$ thin film," in *IOP Conference Series: Earth and Environmental Science*,IOP Publishing, Philadelphia, USA, 2018.

[75] C. Zhang, Z. Ling, and G. Jian, "The defect chemistry and dielectric properties of Sb_2O_3 doped non-stoichiometric barium strontium titanate ceramics," *Journal of Materials Science: Materials in Electronics*, vol. 27, no. 11, pp. 11770–11776, 2016.

[76] M. S. Alkathy, A. Joseph, and K. James Raju, "Dielectric properties of Zr substituted barium strontium titanate," *Materials Today Proceedings*, vol. 3, no. 6, pp. 2321–2328, 2016.

[77] H. W. Wang, S. W. Nien, K. C. Lee, and M. C. Wu, "Improvement in crystallization and electrical properties of barium strontium titanate thin films by gold doping using metal-organic deposition method," *Thin Solid Films*, vol. 489, no. 1-2, pp. 31–36, 2005.

[78] A. Saeed, B. Ruthramurthy, W. H. Yong, O. B. Hoong, T. K. Ban, and Y. H. wang, "Structural and dielectric properties of iron doped barium strontium titanate for storage applications," *Journal of Materials Science: Materials in Electronics*, vol. 26, no. 12, pp. 9859–9864, 2015.

[79] L. Gao, Z. Guan, S. Huang, K. Liang, H. Chen, and J. Zhang, "Enhanced dielectric properties of barium strontium titanate thin films by doping modification," *Journal of Materials Science: Materials in Electronics*, vol. 30, no. 14, pp. 12821–12839, 2019.

[80] M. K. Mahata, T. Koppe, K. Kumar, H. Hofsäss, and U. Vetter, "Upconversion photoluminescence of Ho 3+-Yb 3+ doped barium titanate nanocrystallites: optical tools for structural phase detection and temperature probing," *Scientific Reports*, vol. 10, no. 1, pp. 8775–8812, 2020.

[81] Y. Tsur, T. D. Dunbar, and C. A. Randall, "Crystal and defect chemistry of rare earth cations in BaTiO3," *Journal of Electroceramics*, vol. 7, no. 1, pp. 25–34, 2001.

[82] Y. Tsur, A. Hitomi, I. Scrymgeour, and C. A. Randall, "Site occupancy of rare-earth cations in BaTiO3," *Japanese Journal of Applied Physics*, vol. 40, no. 1R, p. 255, 2001.

[83] M. Jain, S. B. Majumder, R. S. Katiyar, D. C. Agrawal, and A. S. Bhalla, "Dielectric properties of sol–gel-derived MgO: $Ba_{0.5}Sr_{0.5}TiO_3$ thin-film composites," *Applied Physics Letters*, vol. 81, no. 17, pp. 3212–3214, 2002.

[84] J. Liao, X. Wei, Z. Xu, X. Wei, and P. Wang, "The structure and dielectric properties of a novel kind of doped Ba0. 6Sr0. 4TiO3 film," *Materials Chemistry and Physics*, vol. 135, no. 2-3, pp. 1030–1035, 2012.

[85] S. Z. Wang, J. X. Liao, Y. M. Hu, F. Gong, Z. Q. Xu, and M. Q. Wu, "Structures and dielectric performances of Mn/Y alternately doped BST films prepared by a novel preheating process," *Materials Chemistry and Physics*, vol. 193, pp. 50–56, 2017.

[86] W. Q. Cao, F. L. Li, M. M. Ismail, and G. Xiong, "Dielectric properties of Y_2O_3 and Nb_2O_5Co-doped barium titanate ceramics," *Japanese Journal of Applied Physics*, vol. 51, no. 4R, Article ID 041503, 2012.

[87] I. T. Gyoung, S. Baik, and S. Kim, "Leakage current of Al-or Nb-doped $Ba_{0.5}Sr_{0.5}TiO_3$ thin films by rf magnetron sputtering," *Journal of Materials Research*, vol. 13, no. 4, pp. 990–994, 1998.

[88] S. Gopalan, C.-H. Wong, V. Balu et al., "Effect of niobium doping on the microstructure and electrical properties of strontium titanate thin films for semiconductor memory application," *Applied Physics Letters*, vol. 75, no. 14, pp. 2123–2125, 1999.

[89] J. Liao, Z. Xu, X. Wei, X. Wei, P. Wang, and B. Yang, "Influence of preheating on crystallization and growing behavior of Ce and Mn doped $Ba_{0.6}Sr_{0.4}TiO_3$ film by sol–gel method," *Surface and Coatings Technology*, vol. 206, no. 22, pp. 4518–4524, 2012.

[90] L. Yue, W. Cui, S. Zheng, Y. Wu, X. Dong, and G. Lu, "Enhanced thermoelectric performance of in and Se co-doped GeTe compounds," *Journal of Materials Research and Technology*, vol. 9, no. 3, pp. 4106–4113, 2020.

[91] Z. Wang, H. Chen, W. Nian, J. Fan, Y. Li, and X. Wang, "Bismuth oxide modified europium and niobium co-doped titanium dioxide ceramics: colossal permittivity and low dielectric loss design," *Journal of Alloys and Compounds*, vol. 777, pp. 317–324, 2019.

[92] Q. Liu, J. Liu, D. Lu, T. Li, and W. Zheng, "Dense Sm and Mn Co-doped $BaTiO_3$ ceramics with high permittivity," *Materials*, vol. 12, no. 4, p. 678, 2019.

[93] Q. Liu, J. Liu, D. Lu, W. Zheng, and C. Hu, "Structural evolution and dielectric properties of Nd and Mn co-doped $BaTiO_3$ ceramics," *Journal of Alloys and Compounds*, vol. 760, pp. 31–41, 2018.

[94] T. Yamada, H. Takeda, T. Tsurumi, and T. Hoshina, "Possibility of ferroelectric bismuth and nitrogen co-doped barium titanate," *Journal of the Ceramic Society of Japan*, vol. 128, no. 8, pp. 486–491, 2020.

[95] L. M. Zivkovic, V. V. Paunovic, N. L. Stamenkov, and M. M. Miljkovic, "The effect of secondary abnormal grain growth on the dielectric properties of La/Mn co-doped BaTiO3 ceramics," *Science of Sintering*, vol. 38, no. 3, pp. 273–281, 2006.

[96] Z. He, M. Cao, L. Zhou et al., "Origin of low dielectric loss and giant dielectric response in (Nb+ Al) co-doped strontium titanate," *Journal of the American Ceramic Society*, vol. 101, no. 11, pp. 5089–5097, 2018.

[97] W. Dong, J. Liu, S. Li et al., "The dielectric and flexoelectric properties of Mg^{2+}/K^{+} doped BST films," *Ceramics International*, vol. 46, no. 16, pp. 25164–25170, 2020.

[98] J. Qian, C. H. Yang, Y. J. Han, X. S. Sun, and L. X. Chen, "Reduced leakage current, enhanced energy storage and dielectric properties in (Ce, Mn)-codoped $Ba_{0.6}Sr_{0.4}TiO_3$ thin film," *Ceramics International*, vol. 44, no. 17, pp. 20808–20813, 2018.

[99] M. S. Alkathy, K. C. J. Raju, and J. A. Eiras, "Colossal dielectric permittivity and high energy storage efficiency in barium strontium titanate ceramics co-doped with bismuth and lithium," *Journal of Physics D: Applied Physics*, vol. 54, no. 12, Article ID 125501, 2021.

[100] B. Liu, Y. H. Huang, C. C. Hu, K. X. Song, and Y. J. Wu, "Colossal dielectric permittivity in (Al+ Nb) co-doped $Ba_{0.4}Sr_{0.6}TiO_3$ ceramics," *Ceramics International*, vol. 45, no. 11, pp. 14263–14269, 2019.

[101] P. Singh, O. Parkash, and D. Kumar, "Electrical conduction behavior of La and Mn substituted strontium titanate," *Journal of Applied Physics*, vol. 99, no. 12, Article ID 123704, 2006.

[102] F. Alema and K. Pokhodnya, "Dielectric properties of $BaMg_{13}Nb_{23}O_3$ doped $Ba_{0.45}Sr_{0.55}TiO_3$ thin films for tunable microwave applications," *Journal of Advanced Dielectrics*, vol. 05, no. 04, Article ID 1550030, 2015.

[103] F. L. Alema, *Multicomponent Doped Barium Strontium Titanate Thin Films for Tunable Microwave Applications*, North Dakota State University, Fargo, ND 58105, USA, 2014.

[104] B. Stojanović, V. Mastelaro, S. Paiva, and J. Varela, "Structure study of donor doped barium titan ate prepared from citrate solutions," *Science of Sintering*, vol. 36, no. 3, pp. 179–188, 2004.

[105] F. Stemme, M. Bruns, H. Geßwein et al., "Fabrication and characterization of iron and fluorine co-doped BST thin films for microwave applications," *Journal of Materials Science*, vol. 48, no. 9, pp. 3586–3596, 2013.

[106] W. Liu, Y. Lei, W. Feng et al., "Comprehensive dielectric performance of alternately doped BST multilayer films coated with strontium titanate thin layers," *Journal of Materials Research and Technology*, vol. 13, pp. 385–396, 2021.

[107] J. X. Liao, X. B. Wei, Z. Q. Xu, and P. Wang, "Effect of potassium-doped concentration on structures and dielectric performance of barium-strontium-titanate films," *Vacuum*, vol. 107, pp. 291–296, 2014.

[108] H. J. Cho, S. Oh, C. S. Kang et al., "Improvement of leakage current characteristics of $Ba_{0.5}Sr_{0.5}TiO_3$ films by N_2O plasma

surface treatment," *Applied Physics Letters*, vol. 71, no. 22, pp. 3221–3223, 1997.

[109] Y. Zhang, G. Wang, Y. Chen, F. Cao, L. Yang, and X. Dong, "Effect of donor, acceptor, and donor–acceptor codoping on the electrical properties of $Ba_{0.6}Sr_{0.4}TiO_3$ thin films for tunable device applications," *Journal of the American Ceramic Society*, vol. 92, no. 11, pp. 2759–2761, 2009.

[110] C. Gao, X. Huang, J. Yin, M. Huang, and Z. Yue, "Structure and dielectric property of Bi_3NbZrO_9 doped BST ceramics sintered at low temperature," *Ferroelectrics*, vol. 506, no. 1, pp. 32–39, 2017.

[111] Z. Xu, X. Chen, J. Zhu, D. Xiao, and P. Yu, "Effect of annealing temperature on the properties of $Ba_{0.67}Sr_{0.33}TiO_3$: Mn+ Y thin films," *Ferroelectrics*, vol. 446, no. 1, pp. 59–66, 2013.

[112] K. S. Deepa, P. L. Priyatha, P. Parameswaran, M. T. Sebastian, and J. James, "$Ba_{0.7}Sr_{03}TiO_3$–glass–silver percolative composite," *Ceramics International*, vol. 36, no. 1, pp. 75–78, 2010.

[113] P. Bomlai, N. Sirikulrat, A. Brown, E. Condliffe, and S. J. Milne, "Compositional analysis and electrical properties of Sb, Mn-doped barium strontium titanate PTCR ceramics with TiO_2 and SiO_2 sintering additives," *Journal of Materials Science*, vol. 42, no. 6, pp. 2175–2180, 2007.

[114] A. Friederich, X. Zhou, M. Sazegar et al., "The influence of processing on the microstructure and the microwave properties of Co–F-codoped barium strontium titanate thick-films," *Journal of the European Ceramic Society*, vol. 32, no. 4, pp. 875–882, 2012.

[115] H. T. Jiang, J. W. Zhai, J. J. Zhang, and X. Yao, "Dielectric properties and low-temperature sintering of the $Ba_{0.6}Sr_{0.4}TiO_3$ ceramics with B_2O_3/CuO additions," *International Journal of Applied Ceramic Technology*, vol. 10, no. 5, pp. 873–878, 2013.

[116] X. Zhou, H. Geßwein, M. Sazegar et al., "Characterization of metal (Fe, Co, Ni, Cu) and fluorine codoped barium strontium titanate thick-films for microwave applications," *Journal of Electroceramics*, vol. 24, no. 4, pp. 345–354, 2010.

[117] R. H. Liang, X. L. Dong, Y. Chen, F. Cao, and Y. L. Wang, "Effect of various dopants on the tunable and dielectric properties of Ba0. 6Sr0. 4TiO3 ceramics," *Ceramics International*, vol. 31, no. 8, pp. 1097–1101, 2005.

[118] L. Tang, J. Wang, J. Zhai, B. Shen, and X. Yao, "Dielectric tunable properties of $Ba_{0.5}$ $Sr_{0.5}TiO_3$–$MgMoO_4$ composite ceramics for microwave applications," *Journal of Materials Science: Materials in Electronics*, vol. 24, no. 7, pp. 2576–2580, 2013.

[119] D. Zhang, T. W. Button, T. Price, D. K. Iddles, V. O. Sherman, and A. K. Tagantsev, "Effects of glass additions on the microstructure and dielectric properties of barium strontium titanate (BST) ceramics," *Journal of the European Ceramic Society*, vol. 30, no. 2, pp. 407–412, 2010.

[120] J. Zhang, J. Zhai, M. Zhang, P. Qi, X. Yu, and X. Yao, "Structure–dielectric properties relationship in Mg–Mn codoped $Ba_{0.4}Sr_{0.6}TiO_3/MgAl_2O_4$ tunable microwave composite ceramics," *Journal of Physics D: Applied Physics*, vol. 42, no. 7, Article ID 075414, 2009.

[121] D. Yan, Z. Xu, X. Chen, D. Xiao, P. Yu, and J. Zhu, "Microstructure and electrical properties of Mn/Y codoped Ba0. 67Sr0. 33TiO3 ceramics," *Ceramics International*, vol. 38, no. 4, pp. 2785–2791, 2012.

[122] T. Hu, H. Jantunen, A. Uusimäki, and S. Leppävuori, "$Ba_{0.7}Sr_{0.3}TiO_3$ powders with B_2O_3 additive prepared by the sol–gel method for use as microwave material," *Materials Science in Semiconductor Processing*, vol. 5, no. 2-3, pp. 215–221, 2002.

[123] X. Wang, Y. Zhang, Z. Yuan, T. Ma, C. Deng, and X. Dai, "Phase development and dielectric properties of barium strontium titanate based glass ceramics," *Ferroelectrics*, vol. 419, no. 1, pp. 53–58, 2011.

[124] D. Yan, L. Luo, Y. Zhang et al., "Influence of deposition temperature on microstructure and electrical properties of modified (Ba, Sr) TiO_3 ferroelectric thin films," *Ceramics International*, vol. 41, pp. S520–S525, 2015.

[125] W.-B. Li, D. Zhou, and L.-X. Pang, "Structure and energy storage properties of Mn-doped (Ba, Sr) TiO_3–MgO composite ceramics," *Journal of Materials Science: Materials in Electronics*, vol. 28, no. 12, pp. 8749–8754, 2017.

[126] Z. Y. Shen, Y. Wang, Y. Tang et al., "Glass modified barium strontium titanate ceramics for energy storage capacitor at elevated temperatures," *Journal of Materiomics*, vol. 5, no. 4, pp. 641–648, 2019.

[127] Q. Zhang, L. Wang, J. Luo, Q. Tang, and J. Du, "Improved energy storage density in barium strontium titanate by addition of BaO–SiO_2–B_2O_3 glass," *Journal of the American Ceramic Society*, vol. 92, no. 8, pp. 1871–1873, 2009.

[128] M. Vijatović Petrović, J. Bobić, R. Grigalaitis, B. Stojanović, and J. Banys, "La-Doped and La/Mn-co-doped barium titanate ceramics," *Acta Physica Polonica A*, vol. 124, no. 1, pp. 155–160, 2013.

[129] C. Zhang, F. Chen, Z. Ling, G. Jian, and Y. Li, "Microstructure and dielectric properties of La_2O_3 doped Ti-rich barium strontium titanate ceramics for capacitor applications," *Materials Science Poland*, vol. 35, no. 4, pp. 806–815, 2017.

[130] J. Oh, S. . Delprat, M. Ismail, M. Chaker, E. E. Djoumessi, and K. Wu, "Djoumessi &Ke Wu. Improvement of $Ba_{0.5}Sr_{0.5}TiO_3$ thin films microwave properties using codoping with Mg-W and Al-W," *Integrated Ferroelectrics*, vol. 112, no. 1, pp. 24–32, 2010.

[131] M. El-Samanoudy, "Modified Poole–Frenkel mechanisms in $Ge_{25}Bi_xSb_{15-x}S_{60}$ thin films," *Applied Surface Science*, vol. 207, no. 1-4, pp. 219–226, 2003.

[132] S. Y. Wang, B. L. Cheng, C. Wang et al., "Influence of Ce doping on leakage current in $Ba_{0.5}Sr_{0.5}TiO_3$ films," *Journal of Physics D: Applied Physics*, vol. 38, no. 13, pp. 2253–2257, 2005.

[133] J. Ćirković, K. Vojisavljević, N. Nikolić et al., "Dielectric and ferroelectric properties of BST ceramics obtained by a hydrothermally assisted complex polymerization method," *Ceramics International*, vol. 41, no. 9, pp. 11306–11313, 2015.

[134] K. Asa Deepthi, R. Balachandran, B. H. Ong et al., "Physical and electrical characteristics of NiFe thin films using ultrasonic assisted pulse electrodeposition," *Applied Surface Science*, vol. 360, pp. 519–524, 2016.

[135] N. Giridharan, R. Jayavel, and P. Ramasamy, "Structural, morphological and electrical studies on barium strontium titanate thin films prepared by sol-gel technique," *Crystal Research and Technology*, vol. 36, no. 1, pp. 65–72, 2001.

[136] R. Balachandran, H. K. Yow, B. H. Ong, K. Anuar, W. T. Teoh, and K. B. Tan, "Surface morphology and particle size analysis of $Ba_{0.5}Sr_{0.5}$ TiO_3nano-powder grown using sol-gel method," in *Proceedings of the 2008 IEEE International Conference on Semiconductor Electronics*, IEEE, Johor Bahru, Malaysia, November 2008.

[137] A. Saeed, B. Ruthramurthy, T. K. Ban et al., "Structural and magnetic properties of iron doped barium strontium titanate

ceramic synthesised using slow injection sol–gel technique," *Materials Technology*, vol. 30, pp. 140–143, 2015.

[138] R. J. Pandya, U. Joshi, and O. Caltun, "Microstructural and electrical properties of barium strontium titanate and nickel zinc ferrite composites," *Procedia Materials Science*, vol. 10, pp. 168–175, 2015.

[139] B. Li, C. Wang, G. Dou, Z. Wang, and W. Fei, "Crystallized $Bi_{0.9}La_{0.1}Fe_{0.95}Mn_{0.05}O_3/Ba_{0.7}Sr_{0.3}Ti_{0.95}Co_{0.05}O_3$ bilayer thin films with enhanced multiferroic properties," *Applied Surface Science*, vol. 404, pp. 162–167, 2017.

[140] R. Balachandran, B. H. Ong, H. Y. Wong, K. B. Tan, and M. Muhamad Rasat, "Dielectric characteristics of barium strontium titanate based metal insulator metal capacitor for dynamic random access memory cell," *International Journal of Electrochemical Science*, vol. 7, no. 12, Article ID 11895, 2012.

[141] M. A. Shahzad, M. Shahid, I. Bibi et al., "The effect of rare earth Dy^{3+} ions on structural, dielectric and electrical behavior of new nanocrystalline $PbZrO_3$ perovskites," *Ceramics International*, vol. 43, no. 1, pp. 1073–1079, 2017.

[142] A. A. Davtyan, "Proceedings of NAS RA and NPUA : Series of Technical Sciences UDC 537.226:66," vol. 72, p. 102, 2019.

[143] K. H. Ahn, S. Baik, and S. S. Kim, "Significant suppression of leakage current in (Ba, Sr) TiO 3 thin films by Ni or Mn doping," *Journal of Applied Physics*, vol. 92, no. 5, pp. 2651–2654, 2002.

[144] C. S. Hwang, B. T. Lee, C. S. Kang et al., "A comparative study on the electrical conduction mechanisms of $(Ba_{0.5}Sr_{0.5})TiO_3$ thin films on Pt and IrO_2 electrodes," *Journal of Applied Physics*, vol. 83, no. 7, pp. 3703–3713, 1998.

[145] H. Reisinger and R. Stengl, "Fundamental scaling laws of DRAM dielectrics," in *Proceedings of the 2000 Third IEEE International Caracas Conference on Devices, Circuits and Systems (Cat. No. 00TH8474)*, IEEE, Cancun, Mexico, March 2000.

[146] C. Fu, C. Yang, H. Chen, Y. Wang, and L. Hu, "Microstructure and dielectric properties of $Ba_xSr_{1-x}TiO_3$ ceramics," *Materials Science and Engineering: B*, vol. 119, no. 2, pp. 185–188, 2005.

[147] Z. Máté, "Gépjárművek fedélzeti energiatároló rendszerei: on-board energy storage of road vehicles," *Nemzetközi Gépészeti Konferencia–OGÉT*, vol. 1, pp. 255–258, 2021.

[148] C. Basceri, S. K. Streiffer, A. I. Kingon, and R. Waser, "The dielectric response as a function of temperature and film thickness of fiber-textured (Ba, Sr) TiO_3 thin films grown by chemical vapor deposition," *Journal of Applied Physics*, vol. 82, no. 5, pp. 2497–2504, 1997.

[149] M. Dawber, K. M. Rabe, and J. F. Scott, "Physics of thin-film ferroelectric oxides," *Reviews of Modern Physics*, vol. 77, no. 4, pp. 1083–1130, 2005.

[150] K. Hyun Yoon, J. Chan Lee, J. P. Heon Kang, C. Moo Song, and Y. Gyo Seo, "Electrical properties of Mg doped $(Ba_{0.5}Sr_{0.5})TiO_3$ thin films," *Japanese Journal of Applied Physics*, vol. 40, p. 5497, 2001.

[151] Y. H. Huang, Y. J. Wu, J. Li, B. Liu, and X. M. Chen, "Enhanced energy storage properties of barium strontium titanate ceramics prepared by sol-gel method and spark plasma sintering," *Journal of Alloys and Compounds*, vol. 701, pp. 439–446, 2017.

[152] J. Xie, H. Hao, Z. Yao et al., "Energy storage properties of low concentration Fe-doped barium strontium titanate thin films," *Ceramics International*, vol. 44, no. 6, pp. 5867–5873, 2018.

[153] C. Diao, H. Liu, H. Hao, M. Cao, and Z. Yao, "Effect of SiO_2 additive on dielectric response and energy storage performance of $Ba_{0.4}Sr_{0.6}TiO_3$ ceramics," *Ceramics International*, vol. 42, no. 11, pp. 12639–12643, 2016.

[154] S. Yu, C. Zhang, M. Wu, H. Dong, and L. Li, "Ultra-high energy density thin-film capacitors with high power density using $BaSn_{0.15}Ti_{0.85}O_3/Ba_{0.6}Sr_{0.4}TiO_3$ heterostructure thin films," *Journal of Power Sources*, vol. 412, pp. 648–654, 2019.

[155] C. W. Beier, J. M. Sanders, and R. L. Brutchey, "Improved breakdown strength and energy density in thin-film polyimide nanocomposites with small barium strontium titanate nanocrystal fillers," *Journal of Physical Chemistry C*, vol. 117, no. 14, pp. 6958–6965, 2013.

[156] J. D. Baniecki, R. B. Laibowitz, T. M. Shaw et al., "Hydrogen induced tunnel emission in Pt/(Ba_xSr_{1-x}) Ti_{1+y} O_{3+z}/Pt thin film capacitors," *Journal of Applied Physics*, vol. 89, no. 5, pp. 2873–2885, 2001.

[157] M. Izuha, K. Abe, M. Koike, S. Takeno, and N. Fukushima, "Electrical properties and microstructures of Pt/$Ba_{0.5}Sr_{0.5}$ $TiO_3/SrRuO_3$ capacitors," *Applied Physics Letters*, vol. 70, no. 11, pp. 1405–1407, 1997.

[158] E. Ngo, P. C. Joshi, M. W. Cole, and C. W. Hubbard, "Electrophoretic deposition of pure and MgO-modified $Ba_{0.6}Sr_{0.4}TiO_3$ thick films for tunable microwave devices," *Applied Physics Letters*, vol. 79, no. 2, pp. 248–250, 2001.

[159] N. Shaban and M. Bahar, "Synthesis and characterization of Fe and Ni Co-doped $Ba_{0.6}Sr_{0.4}TiO_3$ prepared by Sol-Gel technique," *Journal of Theoretical and Computational Science*, vol. 4, p. 157, 2017.

[160] L. Zhao, Y. Liu, C. Zhai, F. Liao, and Y. Gao, "Photoluminescence properties of Tb-doped and (Zn, Tb) co-doped barium strontium titanate crystalline powders," *Journal of Alloys and Compounds*, vol. 694, pp. 721–725, 2017.

[161] W. Chen, L. Xu, and W. Cao, "Dielectric and ferroelectric characteristics of Ba(1-x)SrxTiO$_3$ ceramics co-doped with Y_2O_3 and Nb_2O_5," *Journal of Hubei University (Natural Science)*, p. 02, 2012.